# Studies on mechanisms of amoeboid locomotion using a novel model system

Yukinori Nishigami

Contents


**Chapter 1** **General Introduction** ····· 2

Figures ····· 5

**Chapter 2** **A Model System of Bleb-driven Amoeboid Locomotion**

2-1 Abstract ····· 7
2-2 Introduction ····· 8
2-3 Materials and Methods ····· 10
2-4 Results and Discussion ····· 13
2-5 Figures ····· 20

**Chapter 3** **A Novel Mechanism of Sol – Gel Conversion in Amoeboid Locomotion**

3-1 Abstract ····· 28
3-2 Introduction ····· 29
3-3 Materials and Methods ····· 31
3-4 Results and Discussion ····· 33
3-5 Figures ····· 37

**Chapter 4** **Effects of Calcium Ion on Amoeboid Motion in the Model System and the Living Cell**

4-1 Abstract ····· 44
4-2 Introduction ····· 45
4-3 Materials and Methods ····· 47
4-4 Results and Discussion ····· 50
4-5 Figures ····· 53

**Chapter 5** **An Attempt to Make an Additional Model System, Which Is Enclosed by Membrane**

5-1 Abstract ····· 58
5-2 Introduction ····· 59
5-3 Materials and Methods ····· 60
5-4 Results and Discussion ····· 62
5-5 Figures ····· 64

**Chapter 6** **General Discussion** ····· 66

**References** ····· 69

**Acknowledgement** ····· 80

## Chapter 1

## General Introduction

Amoeboid movement is important in many types of life activities, e.g., cell locomotion during developments (Blaser *et al.*, 2006), remodeling and regeneration of damaged tissue (Zhao, 2009), cancer metastasis (Olson & Sahai, 2009), cell locomotion of free-living amoeba (Stockem & Klopocka, 1988) and so on. Since the development of microscopy, people have been fascinated by the dynamic movement of giant amoebae, and the mechanism underlying this movement has been extensively studied. About 50 years ago, two hypotheses, called the front-contraction and tail-contraction hypotheses, were proposed to explain the origin of the motive force of amoeboid movement. The former posited that serial structures in the cytoplasm are pulled by contraction at the sol-gel transition region at the extending pseudopod (Allen, 1961; Allen *et al.*, 1960; Figure 1A). The latter insisted that the cytoplasm is extruded by hydrostatic pressure caused by contraction of the posterior gel layer (Goldacre & Lorch, 1950; Goldacre, 1956, 1961, 1964; Jahn, 1964; Marsland, 1956; Mast, 1923, 1926; Rinaldi & Jahn, 1963; Rinaldi *et al.*, 1975) or cell cortex (Grebecki, 1978, 1982; Figure 1B). Although many experiments supported the tail-contraction hypothesis (Goldacre & Lorch, 1950; Goldacre, 1956, 1961, 1964; Jahn, 1964; Kawakatsu *et al.*, 2000; Marsland, 1956; Mast, 1923, 1926; Oh & Jeon, 1998; Rinaldi & Jahn, 1963; Rinaldi *et al.*, 1975; Stockem *et al.*, 1982, 1984; Taylor *et al.*, 1980b; Yanai *et al.*, 1996), the hypothesis could not explain the Allen's observations (Allen, 1961; Allen *et al.*, 1960), which supported front-contraction hypothesis. In his experiments demembraned cell cytoplasm moved in grass capillary despite the fact that the demembraned system

would not produce hydrostatic pressure. Hence, this controversy subsided with no evident conclusion. In recent studies of keratocytes, mammalian cultured cells and social amoeba, but not giant amoeba, it is generally accepted that the pseudopod extension is caused by actin polymerization in the anterior region (Mitchison & Cramer, 1996; Parent, 2004; Pollard & Borisy, 2003; Figure 2A). Recently, the importance of intracellular pressure caused by contraction of the cortex in the extending pseudopod has been proposed in a variety of cell types including mammalian cultured cells (Charras, 2008; Fackler & Grosse, 2008) and social amoeba, *Dictyostelium discondium* (Yoshida & Soldati, 2006). This type of amoeboid locomotion is called bleb-driven amoeboid locomotion (Figure 2B), and this type of locomotion is thought to have a similar mechanism to the above-mentioned tail-contraction hypothesis. In many biological phenomena, this bleb-driven type locomotion is important, however, the mechanism underlying amoeboid movement is still unclear. One reason is that most of the cells, which show bleb-driven amoeboid locomotion, exhibit both bleb-driven and actin polymerization mode locomotion depending on extracellular conditions. Another reason is the complexity of bleb-driven amoeboid locomotion. To elucidate the mechanism underlying cell motility, I used *Amoeba proteus*, which is considered to move always using bleb-driven mode, and tried to make a novel model system to simplify the complexity of the cell. In giant amoeba, whole cell contraction and cytoplasmic streaming were reported in glycerinated models (Kuroda & Sonobe, 1981; Rinaldi & Opas, 1978; Taylor *et al.*, 1980). However, their movements were far from the pattern observed in living cells. Allen reported protrusion of the pseudopod and cytoplasmic streaming in a mechanically demembraned model (Allen, 1961; Allen *et*

*al.*, 1960), supporting the front-contraction hypothesis. However, these experimental model systems are not suitable for further analyses, because the model systems are too complex to exchange the components of the model systems. In this thesis, I sought to make a novel contorollable model system and succeeded in reconstituting bleb-driven amoeboid locomotion *in vitro* with fractionated components prepared from amoeba cells. In addition, I used the model system to elucidate mechanism of cytoplasmic sol-gel conversion and importance of calcium ion during cell locomotion.

**Figures**

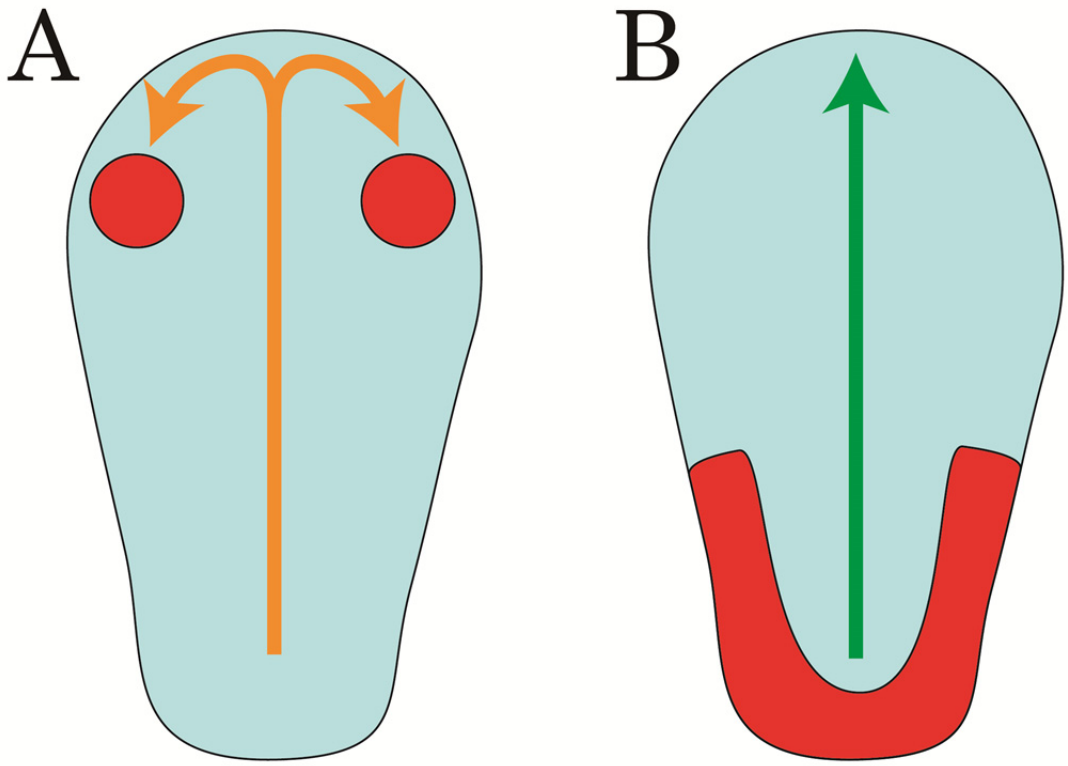


**Figure1. Two alternative hypotheses of the mechanism of giant free-living amoeba locomotion.** To explain the origin of the motive force of amoeboid movement of giant free-living amoeba, two hypotheses, called the front-contraction hypothesis (A) and tail-contraction hypothesis (B), have been proposed. The front-contraction hypothesis posited that serial structures in the cytoplasm are pulled by contraction at the sol-gel transition region at the extending pseudopod (red color region in A). The tail- contraction hypothesis insisted that the cytoplasm is extruded by hydrostatic pressure caused by contraction of the posterior gel layer (red color region in B) or cell cortex.

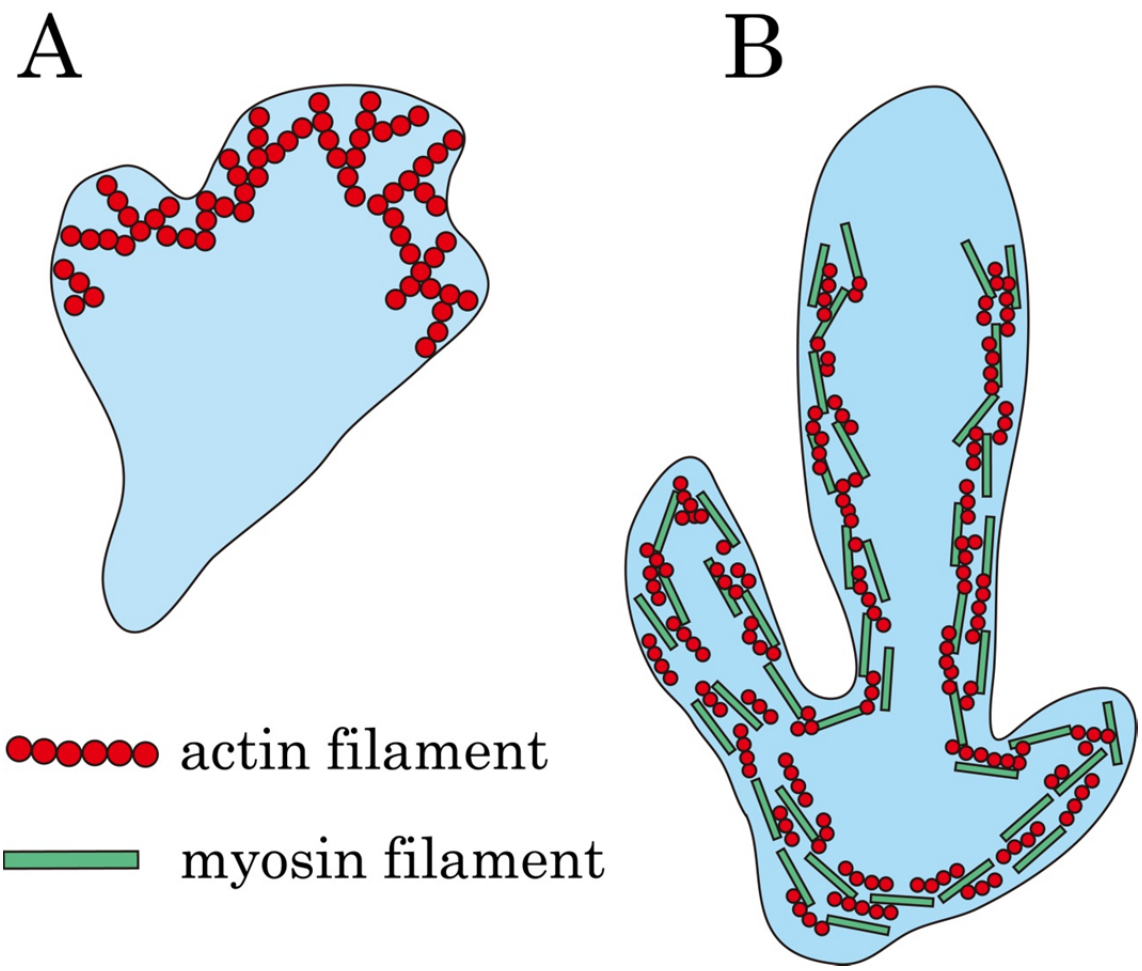


**Figure 2. Two modes of amoeboid locomotion.** It is generally accepted that the pseudopod extension is caused by actin polymerization in the anterior region (A). Recently the importance of intracellular pressure caused by contraction of the cortex in the extending pseudopod has been proposed (B). This type of amoeboid locomotion called bleb-driven amoeboid locomotion, and this type of locomotion is thought to have a similar mechanism to the above-mentioned tail-contraction hypothesis.

## Chapter 2

## A Model System of Bleb-driven Amoeboid Locomotion

### 2-1 Abstract

The mechanism of bleb-driven amoeboid locomotion is still unclear, because of the complexity of cells, which have many functions to live. I have succeeded in reconstituting bleb-driven amoeboid locomotion *in vitro*, in which system the complexity was reduced. From the several results of experiments, the measured parameters in force generation and new pseudopod formation were similar to those of the living cell. Especially, strength of the force generated in this *in vitro* model system is in the order of magnitude similar to that generated *in vivo*. From these results, I conclude that the novel system reproduces amoeboid locomotion by the mechanism to that operating in the living amoeba.

## 2-2 Introduction

Amoeboid locomotion, the most typical mode of locomotion in adherent eukaryotic cells, appears in a variety of biological processes such as embryonic development (Blaser *et al.*, 2006), wound healing (Zhao, 2009), cancer metastasis (Olson & Sahai, 2009) and so on. It is generally accepted that actin polymerization in the elongating part generates a direct driving force in locomotion (Pollard & Borisy, 2003). Recently, however, the amoeboid locomotion mechanism "bleb-driven amoeboid locomotion" has been proposed (Charras & Paluch, 2008; Fackler & Frosse, 2008), in which the cell cortex actomyosin contracts to increase hydrostatic pressure inside the cell, and a part of the cell cortex is broken to form protrusion in the desired direction of flow. This type of amoeboid locomotion has been recognized in many cell types during cell migration especially within a three-dimensional matrix *in vitro* or tissue *in vivo* (reviewed by Charras & Paluch, 2008). Despite keen interest in bleb-driven amoeboid locomotion, its mechanistic basis remains unclear because of the complexity of bleb-driven amoeboid locomotion.

Reconstitution approaches have been adopted to understand complex biological phenomena such as the cell cycle (Murray & Kirschner, 1989), mitotic spindle assembly (Heald *et al.*, 1996), eukaryotic cilia and flagella beating (Sanchez *et al.*, 2011), filopodia elongation (Lee *et al.* 2010), *etc.* However, bleb-driven amoeboid locomotion has never been reconstituted *in vitro*. Therefore, I sought to develop a novel model system that has the essence of bleb-driven amoeboid locomotion.

In this chapter, I report the reconstitution of bleb-driven amoeboid locomotion using a crude cytoplasmic extract and an actomyosin fraction from

*Amoeba proteus* (Figure. 1 and Figure. 2) and clarify the similarity between locomotion in the reconstitution model system and that in the living cell.

## 2-3 Materials and Methods

### Cell culture

Mass culture of *Amoeba proteus* was performed as described previously (Nishihara *et al.*, 2008). In brief, *Amoeba proteus* was cultured in the KCM medium (7 mg/l KCl, 8 mg/l $CaCl_2$, and 8 mg/l $MgSO_4 \cdot 7H_2O$) at 25°C and fed with *Tetrahymena pyriformis*. Cells were starved for at least 2 days before use to avoid contamination with *T. pyriformis*.

### Preparation of the *in vitro* amoeba (IVA) system

All preparations were at 2°C carried out, and movement was observed at room temperature. Ten grams of *A. proteus* was suspended in an EMP solution (2 mM *O,O'-Bis*(2-aminoethyl)ethyleneglycol-*N,N,N',N'*-tetraacetic acid (EGTA), 2 mM $MgCl_2$, 20 mM Piperazine-1,4-*bis*(2-ethanesulfonic acid) (PIPES) -KOH, pH 7.0) and centrifuged at 6,000 × *g* for 2 min and after removed the supernatant. Then obtained precipitate was centrifuged at 600,000 × *g* for 20 min to obtain a cytoplasmic extract. The precipitate was suspended in a 3 M KCl solution (3 M KCl, 2 mM $MgCl_2$, 1 mM threo-1,4,-dimercapto-2,3-butanediol (DTT), 20 µg/ml leupeptin, 20 µg/ml pepstatin A, 20 mM imidazole-HCl, pH 7.0) and centrifuged at 400,000 × *g* for 10 min. The resultant supernatant was dialyzed against 50 mM KCl, 2 mM EGTA, 2 mM $MgCl_2$, 1 mM DTT, 0.2 mM adenosine-5'-triphosphate (ATP), 20 mM imidazole-HCl, pH 7.0 for 5 h. Actomyosin was collected by centrifugation at 20,000 × *g* for 5 min and suspended in a 150 µl EMP buffer containing 1 mM DTT to prepare an actomyosin fraction. ATP at a final concentration of 2 mM was added to either the amoeba extract or the actomyosin fraction or both. Concentrations of

proteins in both the fractions were determined by the method of Bradford with bovine serum albumin as a standard, and the concentrations of both were approximately 20 mg/ml. One microliter of the actomyosin fraction was injected into 10 µl of the cytosolic extract on a coverslip. Movement was observed by a stereomicroscope (SZH, Olympus, Tokyo, Japan) with dark-field illumination and recorded by a CCD camera (KY-F550, Victor, Tokyo, Japan).

### Treatment with inhibitors

To examine the effects of inhibitors, either 5 µM latrunculin B, 30 µM cytochalasin D, or 100 mM 2,3-butanedione monoxime was added to both fractions on ice with 0.1% dimethyl sulfoxide (DMSO) and allowed to stand for 15 min before injection. A circularity ratio was calculated by length of boundary surface and area of actomyosin fraction using ImageJ and Igor 6.22A (WaveMetrics, Portland, OR, USA).

### Electron microscopy

For electron microscopy, 1 µl of the actomyosin fraction into 10 µl of the cytoplasmic extract in a test tube, and the assay mixture was carefully mixed with 1 ml of a fixative solution (10% glutaraldehyde, 0.5% tannic acid, and 50 mM cacodylate buffer (sodium cacodylate - HCl, pH 7.0). The samples were postfixed with 2% $OsO_4$ in a cacodylate buffer (50mM, pH 7.0) for 1 h, dehydrated, and embedded in Spurr's resin. Ultrathin sections were prepared with ultramicrotome (Reichert-Nissei Ultracut S, Laica Microsystems, Wetzlar, Germany), stained with

uranyl acetate and lead citrate and observed using an electron microscope (JEM 1200 EX, JOEL, Tokyo, Japan).

### Fluorescence time-laps imaging

To reveal the distribution of actin in the IVA system, the cytosolic extract and actomyosin fraction was stained with Alexa Flour 488-phalloidin (Invitrogen, Carlsbad, CA, USA). Time-laps Images were taken by a stereomicroscope (MZ 16F, Leica Microsystems) equipped with a CCD camera (DP72, Olympus).

### Statistical analysis.

Statistical analysis was carried out using Igor 6.22A (WaveMetri34cs, USA).

## 2-4 Results and Discussion

To prepare an model system of bleb-driven amoeboid locomotion packed *A. proteus* cells were ultracentrifuged and cytoplasmic extract was obtained. Because most myosin II is present in thick filament (Sonobe & Kuroda, 1986), the extract contained little myosin II (Figures. 3A and B); on the other hand, this protein was abundant in the pellet following high-speed centrifugation. The pellet was extracted with a high-salt solution and the eluate was dialyzed to form myosin II thick filaments. Filaments were collected by centrifugation and suspended in the EMP solution to obtain the "actomyosin fraction." The cytosolic extract was rich in actin and poor in myosin, whereas the actomyosin fraction was rich in myosin with moderate actin (Figure. 3A, B and C). Injection of the actomyosin fraction into the cytosolic extract induced vigorous locomotion (Figure. 1A & Figure. 2). The boundary between the injected actomyosin fraction and the surrounding cytosolic extract bulged to form a sphere. Contents of the spheroidal actomyosin body effused into the surrounding cytosolic extract from a hole in the boundary, forming a new surface structure on the boundary. Sequential repetition of this contraction and effusion produced locomotion similar to bleb-driven amoeboid locomotion. No movement was observed when the cytosolic extract was replaced with a protein-free buffer (data not shown), suggesting that both fractions are required for this amoeboid-like locomotion. This experimental model system was named the "*in vitro* amoeba" (IVA) system.

Analogous consideration of spherical droplet formation suggests the presence of a membrane-like structure on the boundary and emergence of surface tension. To reveal boundary surface composition, I fixed the preparation just before

first effusion of the actomyosin body contents and examined it by electron microscopy. The body of the myosin fraction was covered by an electron-dense interface, which appeared to comprise highly aggregated actin and myosin (Figure. 3D and E). Time lapse fluorescent image of actin in IVA revealed that actin was accumulated at the boundary surface (Figure. 4), suggesting that the motive force of the IVA system was generated at the actomyosin cortex. To confirm the involvement of actomyosin contraction in IVA system movement, it was treated with latrunculin B or cytochalasin D, inhibitors of actin polymerization, or with a myosin inhibitor 2,3-butanedione monoxime (BDM); marked motility inhibition was observed (Figure. 5). Therefore, surface contraction was produced by a dense membrane-like structure consisted of randomly interwoven actomyosin. It is reasonable that the motility of IVA system should depend on the contraction of surface actomyosin, but a possibility that actin dynamics, polymerization and depolymerization, might partly take part in motive force generation cannot be completely excluded. The tension-exerting surface or cortex is similar to that of other actomyosin systems (Ishiwata & Yasuda, 1993; Takiguchi, 1991). In addition to force generation of the surface actomyosin contraction in IVA system, a part of the boundary surface actin was broken (arrow head in Figure 4), and the actomyosin body contents effused into the surrounding cytosolic extract from the broken boundary surface at the time of forming a new pseudopod like structure. These processes of making the pseudopod-like structure are similar to that of forming a new pseudopod in the cell performing the bleb-driven locomotion (Charras & Paluch, 2008; Fackler & Frosse, 2008). From these observations, the IVA system seems to use mechanisms similar to those of the bleb-driven or tail-contraction locomotion.

As mentioned in Chapter 1, Allen denied tail-contraction hypothesis, because, in his experiments, the demembraned cell cytoplasm moved in glass capillary despite the fact that the demembraned system would not produce hydrostatic pressure (Allen, 1961; Allen *et al.*, 1960). In the IVA system, moving actomyosin fraction was not enclosed by any membrane (Figure 3D), however, actomyosin fraction could move like amoeba. This phenomenon indicated that highly aggregated actomyosin restrains free dissipation of water, and produce some hydrostatic pressure even in the absence of the membrane. Therefore, I conclude that, Allen's argument is irrelevant.

A newly formed pseudopod-like structure passed through the following four stages (Figure. 6): expansion, contraction-without-elution, resting, and contraction-with-elution. In the expanding stage, the actomyosin enclosed by the contracting actomyosin boundary surface flowed into a new pseudopod-like structure. In the contraction-without-elution stage, the effused actomyosin formed a new boundary surface on the cytoplasmic extract and started contracting. With the cortex restricting the flux of actomyosin fraction beyond the boundary, coalescence of the cortices along the boundary generated hydrostatic pressure within the actomyosin fraction. In the resting stage, internal hydrostatic pressure was equal to surface contraction force generated by the actomyosin contraction at the boundary surface, ambient pressure, gravity-generated forces and so on. The round-shaped IVA system shrank to a sphere. During contraction-with-elution, a weak region of the interface ruptured spontaneously, resulting in effusion of the internal actomyosin fraction into the external cytosolic extract.

The amoeba-derived system reconstituted an amoeboid migration type through pseudopod elongation. Pseudopod-driven locomotion resembles bleb-driven locomotion phenomenologically. Repeated IVA contraction and effusion is similar to oscillatory motion of a bleb in a fibroblast and its fragments (Palch *et al.*, 2005). Both dynamics were driven by the contractile nature of the active actomyosin cortex, confirmed by the actin and myosin inhibitor treatments, respectively (Figure. 5). IVA is the simplest system for cell blebbing and locomotion (Palch *et al.*, 2006). However, there are several differences between the IVA system and previous bleb systems (Palch *et al.*, 2005; Charras *et al.*, 2005; Charras *et al.*, 2006; Tinevez *et al.*, 2009), such as a larger scale, higher flow speed, and more vigorous motion. I briefly discuss the characteristic motions of the IVA for defining the fundamental features of the movement of the IVA system.

In expanding and contracting without elution stages, the actomyosin body was transformed from an amorphous shape to a spherical shape, indicating that the generated cortical tension made it spherical. Accordingly, slight shrinking in resting stage reflects transformation from a distorted sphere to sphere. When these conditions where a small morphological change occurs, the Mahadevan–Pomeau model can be applied to estimate surface tension (Mahacevan & Pomeau, 1999), which is based on $\Delta S \propto 1/\gamma^2$ , where $\Delta S$ is the deviation of the surface area from that of a sphere, and $\gamma$ is the total surface tension, including cortical tension and counteracting Young forces from the droplet body and cortex (Paluch *et al.*, 2006; Tinevez *et al.*, 2009; van der Gucht & Sykes, 2009). The model indicates that the total surface tension on the actomyosin body increased in resting stage (Figure. 7A), and contraction-without-elution stage began when the increasing inner pressure

exceeded the breaking strength of the actomyosin cortex on the surface (van der Gucht & Sykes, 2009).

In the contraction-with-elution stage, if the bulge and original actomyosin body were static, a Laplace-type pressure balance equation could be applied (Mahacevan & Pomeau, 1999; Tinevez *et al.*, 2009); however, the elution is not static. Accordingly, a dissipation balance was applied for estimating time differentiation values of cortical tension. The dissipation on the droplet surface can be approximated as $\sim \frac{\partial s}{\partial t}\gamma = \frac{2}{R}\frac{\partial V}{\partial t}\gamma$, where $R$, $s$ and $V$ are radius, surface area, and volume of the droplet, respectively. This surface tension is assumed to be used in hydrodynamic dissipation as $\sim \eta\left(\frac{\partial v}{\partial r}\right)^2 V_{total}$ (Goldstein *et al.*, 2001), where $\eta$ is the viscosity and $V_{total}$ is the total flowing volume, which can be approximated as the conserved total actomyosin volume. Under a linear approximation, the shear strength $\frac{\partial v}{\partial r}$ is proportional to the flow speed $v$. The flow speed may be expressed by shear strength at the effusion hole of which area is $S_{hole}$ as $v \sim \frac{1}{S_{hole}}\frac{\partial V}{\partial t}$. The qualitative balance $\frac{2}{R}\frac{\partial V}{\partial t}\gamma \propto \eta\left(\frac{1}{S_{hole}}\frac{\partial V}{\partial t}\right)^2 V_{total}$ leads to the simple relation $\gamma \propto R\left(\frac{\partial V}{\partial t}\right)$. (Eq. 1)

Figure 7B shows the time development of droplet volume measured from the projected droplet area. The experiments exhibit $dV/dt$ decaying with $t^{\alpha}$, where $\alpha$ is approximately −1 in this limiting case. Figures 7C and D show the qualitative behavior of total surface tension $\gamma$ calculated from the experimental data using the

equations 1. The surface tension decayed but persisted during shrinking. For the order estimation of the tension, if viscosity $\eta$ exhibits the same value of water, the shear strength $\frac{\partial v}{\partial r} \sim 1$ [$s^{-1}$] results in ~ 20 μN/m in surface tension, which was one order of magnitude larger than that in Figure. 7A. From this order estimation and the fact that the actomyosin viscosity was quite high, e.g., 4.5mPa·s in cytoplasmic sol *in vivo* (Rogers *et al.*, 2008) and ~ 100 mPa·s in a F-action solution (Kunita *et al.*, 2012), it can be supposed that almost all the contractive force of the boundary surface was used for deforming own body, and the part of the stored elastic energy was relieved from the rupture as the protrusion. In this geometry, Young's modulus of the inner droplet part has relatively lower value than that of cortex because of the continuous flow, and Young's modulus of cortex is approximated as $\sim E_c\left(\frac{h}{R}\right)$, where $h$ is the thickness of the cortex respectively (Tinevez *et al.*, 2009). In the early effusion stage, the Young's modulus of cortex can be assumed to be lower than that in late stage. Although $h$ could not be measured, the empty shell exhibited a rather thick cortex with buckling. $h/R$ should be considerable in the late contraction stage. Relative value of surface tension decreased with constant tendency (Figure 7C); however, the decay exhibited rapid decrease rather than $\sim -1/R$, which is decay of ideal elastic body. Thus, Figure 7C and D indicate that the actomyosin gel cortex continuously contributed to contraction even after initial relaxation. A static or small bleb may originate in compressive elasticity of the boundary surface. The elastic surface was compressed to the point of pressure equalization, while the incompressible solution leaked out as a new pseudopod-like structure. This balance generated a static or small bleb. However, when the

actomyosin body had a nearly sol constitution or non-elastic response in the deformation time scale, the above mentioned balance among surface force, Laplace pressure and Young's moduli of the inside and the cortex will be broken to take either stationary or effusing (Paluch *et al.*, 2006). Because some experiments exhibited no effusion, the Young's modulus could sometimes afford sufficient antagonistic force against cortical tension; however, the cortex thickness and modulus were still uncontrolled. The elastic response or flowability of the inner part plays an important role in generating amoeboid locomotion from blebbing. How IVA acquire adaptive flowability remains to be clarified. From these observations, I conclude that IVA system is similar to bleb-driven locomotion cells in the mechanism of driving-force generation.

## 2-5 Figures

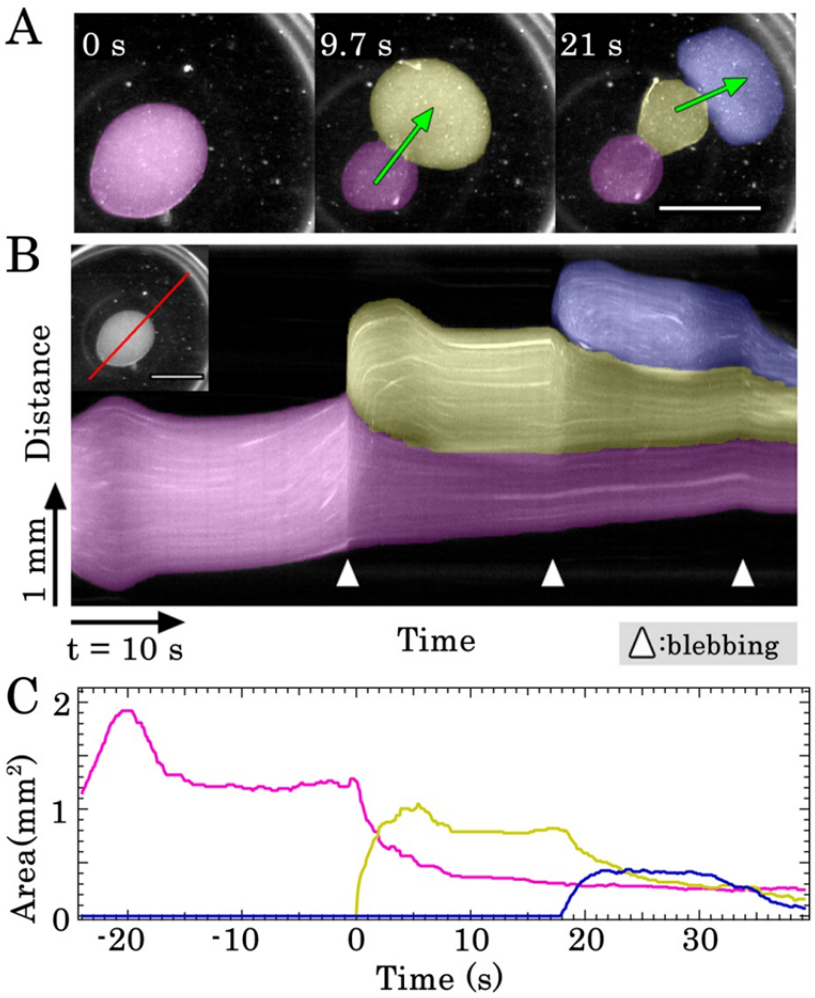


**Figure 1. Observation of the *in vitro* amoeba (IVA) system.** (A) On injecting the actomyosin fraction (pseudocolor) into the cytosolic extract (clear region), the actomyosin fraction showed movement resembling bleb-driven amoeboid locomotion. Scale bar, 1 mm. (B) A kymograph of a moving IVA system. A red line on left upper panel indicates a region used for the kymograph. Arrow heads are the time of starting pseudopod like structure. Zero second is the time of starting to form first pseudopod-like structure. Scale bar, 1 mm. (C) Temporal changes in each pseudopod-like structure areas. Colors of line correspond to those in (A) and (B).

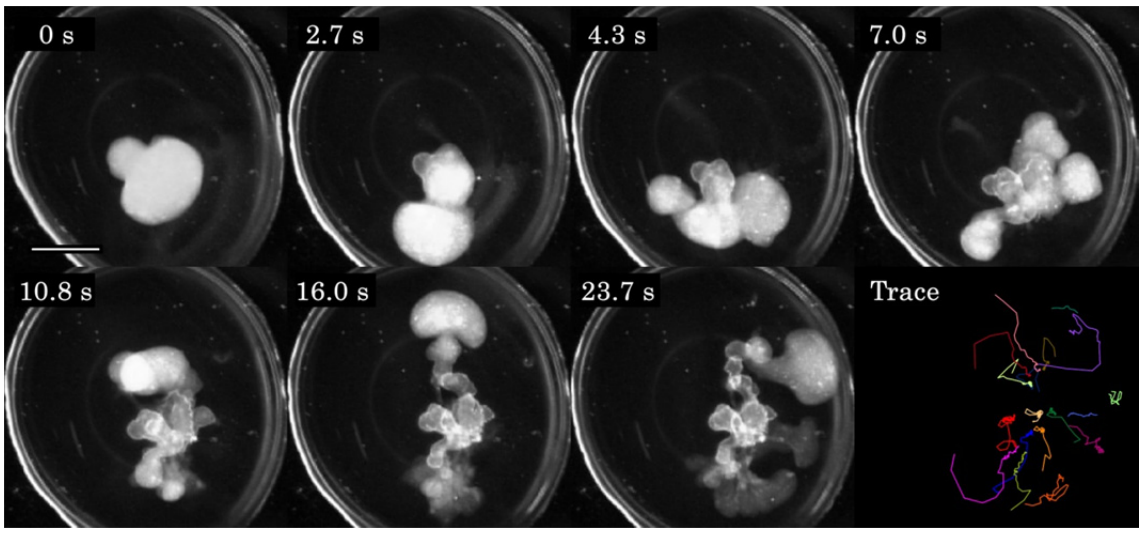


**Figure 2. Locomotion of the IVA system.** Time-lapse image of the of the IVA system are shown from time = 0 s to time = 23.7s. In this time, trajectories of center of mass of each pseudopod-like structure are shown in right lower panel. The period of elution and contraction cycle is between ~1 s to 30 s in IVA system (also see Figure 1). Scale bar, 1 mm.

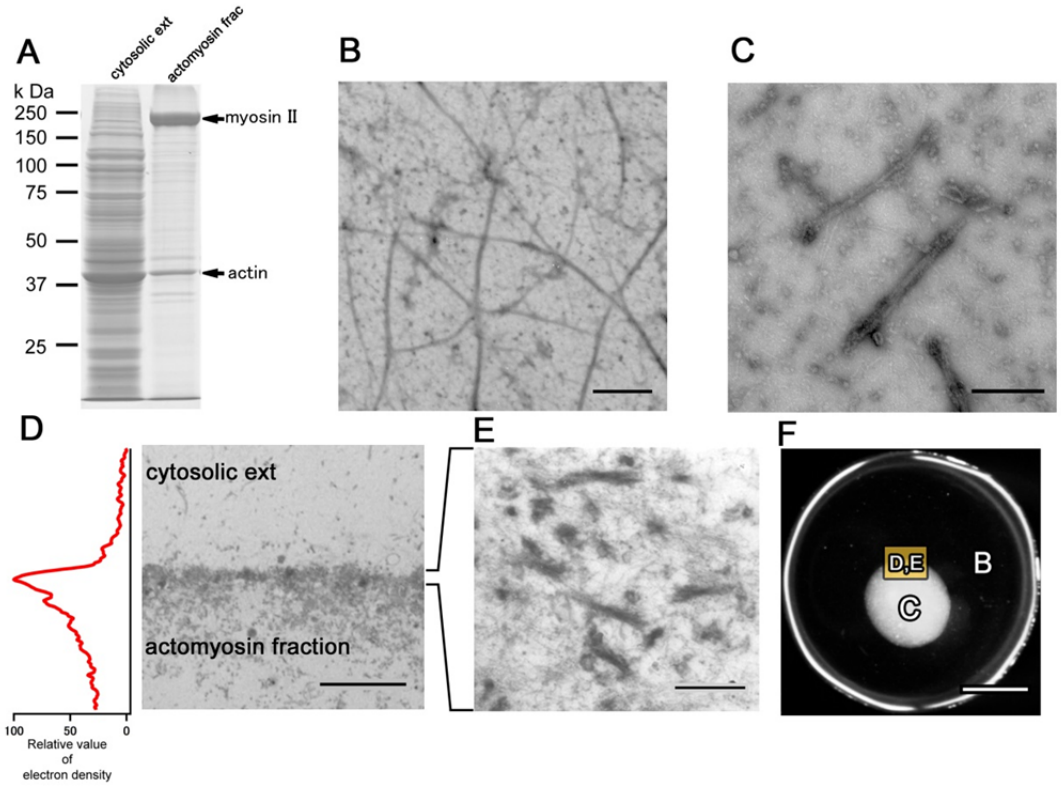


**Figure 3. Components of the IVA system.** (A) The cytosolic extract and the actomyosin fraction for the IVA system were analyzed by SDS-PAGE. The upper arrow indicates the protein band corresponding to myosin II and lower does actin. (B) An electron micrograph showing single actin filaments (arrow) and bundle actin filaments (arrow head) in the cytosolic extract. Samples were negatively stained with 2% uranyl acetate. Scale bar, 1 μm. (C) An electron micrograph showing actin filaments (arrow) and myosin filaments (arrow head) in the actomyosin fraction. Scale bar, 200 nm. (D) An electron micrograph showing that the interface between the cytosolic extract and myosin fraction comprises an electron-dense structure. Scale bar, 5 μm. Relative value of electron density of right panel shows as left one. (E) At higher magnification, the boundary surface appears to comprise highly aggregated actin and myosin. Scale bar, 250 nm. (F) Low-magnification image showing regions in each Figure. Scale bar, 1 mm.

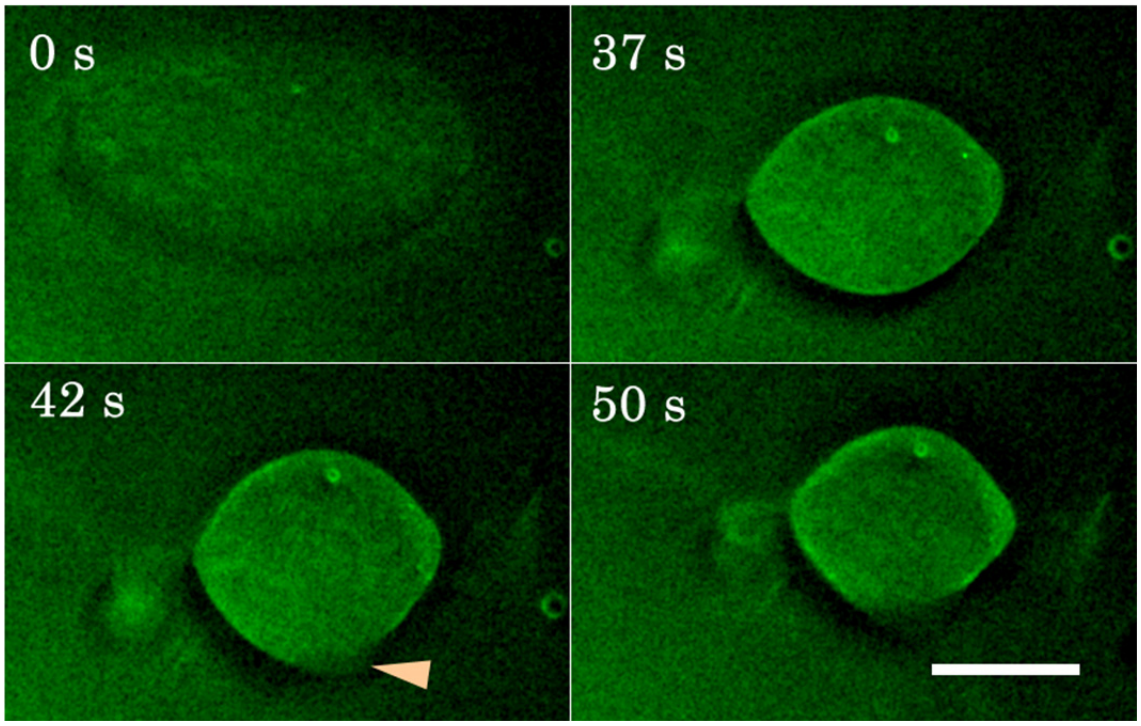


**Figure 4. Distribution of actin in the IVA system.** Distribution of actin filaments were visualized by staining with Alexa 488- phalloidin and monitored by time-lapse observation under the fluorescent microscope. At the time of forming a new pseudopod-like structure (42 s), a part of the boundary surface actin was broken (arrow head) and actomyosin body content effused into the surrounding cytosolic extract from the broken boundary surface. Scale bar, 500 μm.

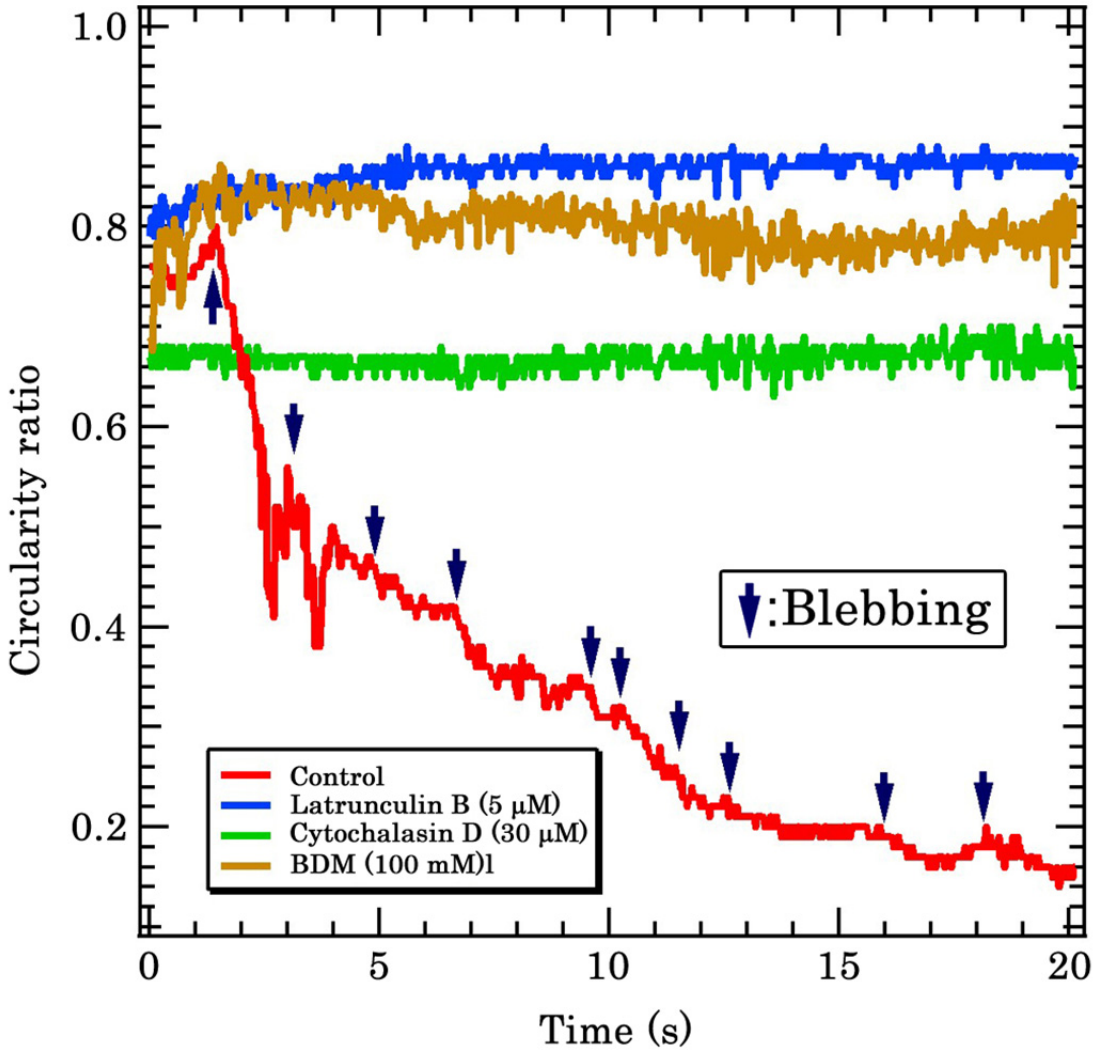


**Figure 5. Inhibition of the IVA system movement by various drugs affecting the actomyosin system.** The IVA system was treated with inhibitors for actin or myosin. The longitudinal axis represents the value of circularity ratio, of which the movement accompanies decrease. Arrows indicate the time of formation of new pseudopod-like structures. The experiments were repeated at least six times, yielding essentially identical results. One typical example of individual inhibitors is shown in the Figure.

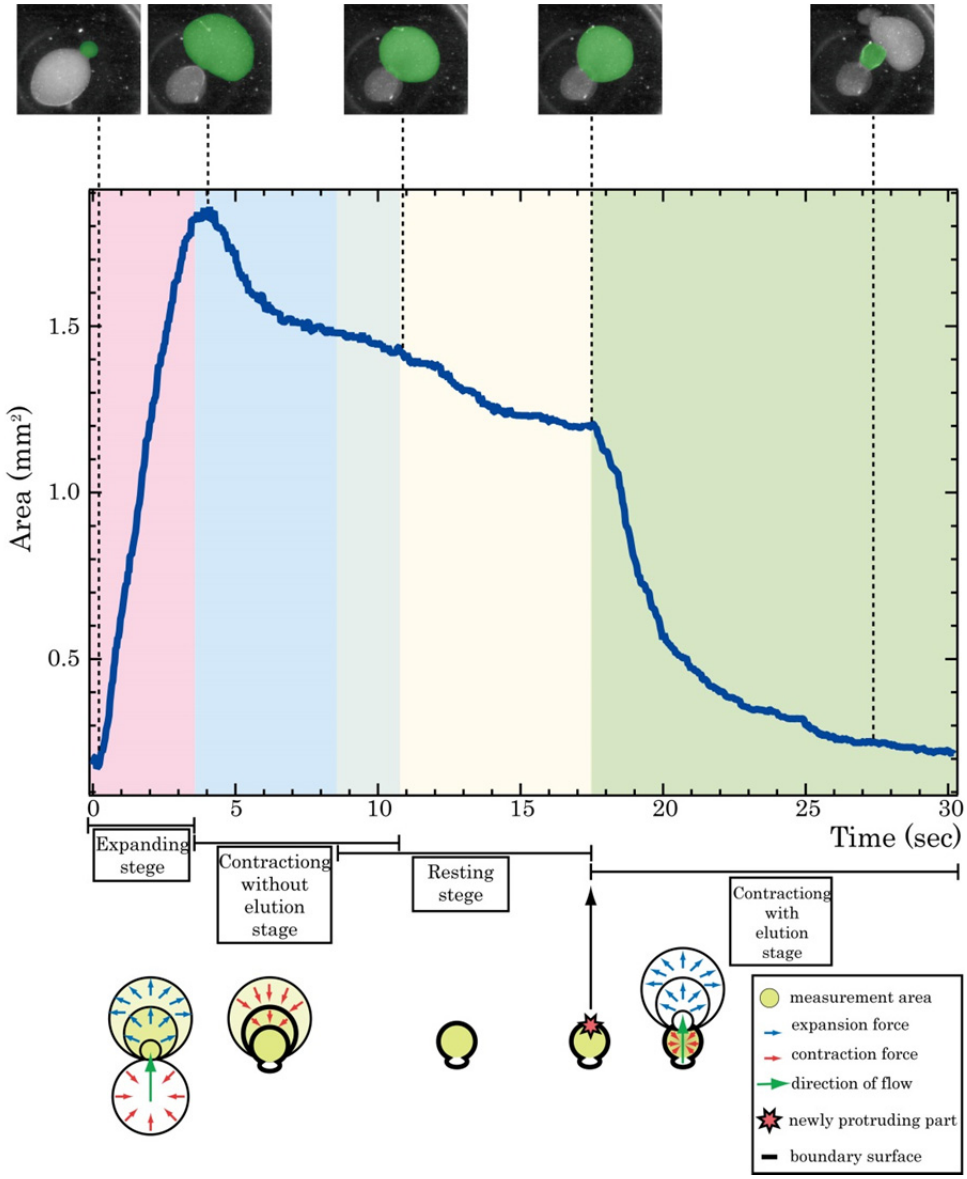


**Figure 6. Four stages in pseudopod-like structure dynamics.** The graph shows the size change of pseudopod-like structure represented by the area in the microscopic images, which is shown in the upper real image and the lower diagram. Dynamics of the pseudopod-like structure is split into four stages of activity: expanding, contracting without elution, resting, and contracting with elution. In the lower schematic diagram, Yellow-green area represents measurement area. The arrows

colored with blue, red or green represent expansion force, contraction force or direction of flow respectively. The red star represents the part in which boundary surface (thick line) is broken.

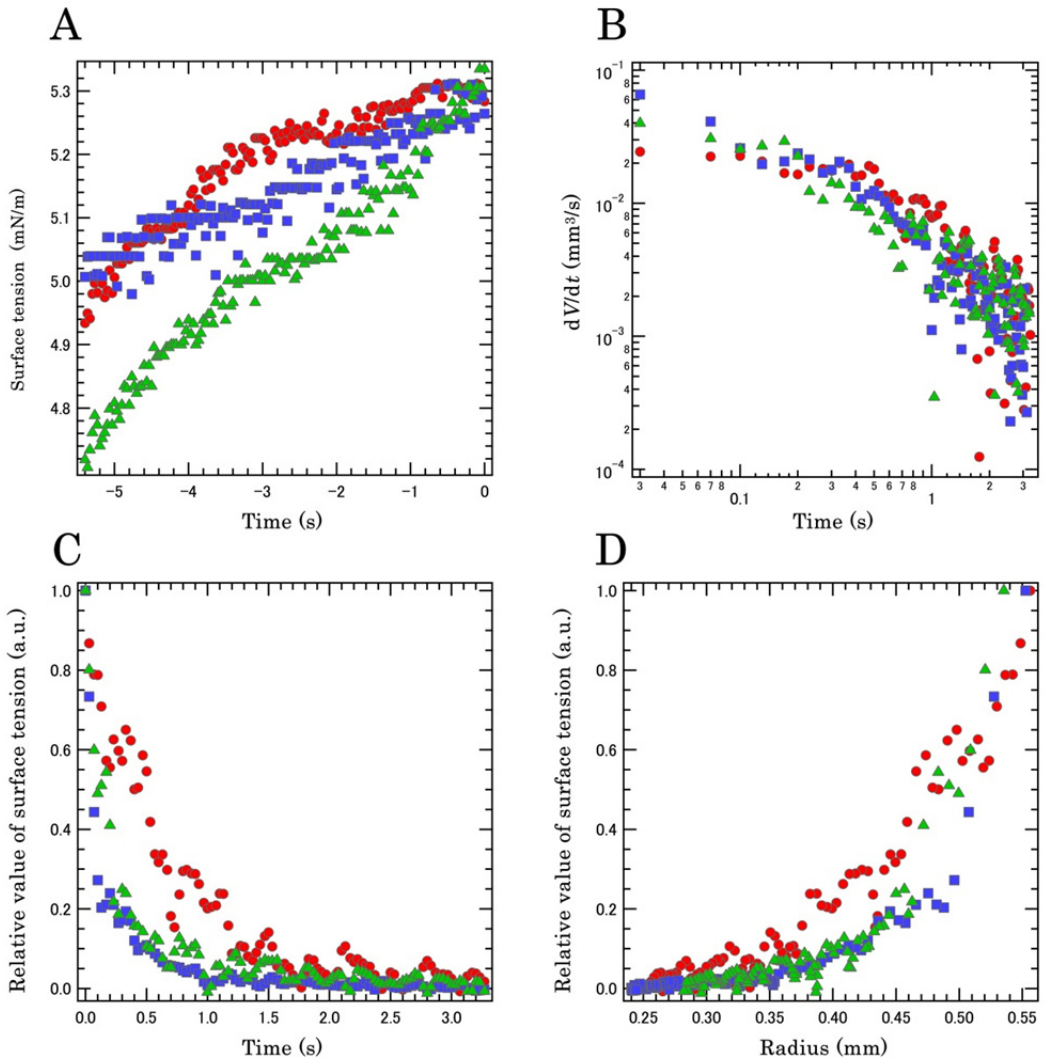


**Figure 7. Surface tension in the IVA system.** (A) Temporal change of surface tension in resting stage. (B) Relationship between time differentiation values of volume and time in the contraction-with-elution stage. (C) Relationship between relative value of surface tension and time in the contraction-with-elution stage. (D) Relationship between relative value of surface tension and radius of actomyosin body in the contraction-with-elution stage. In all panels, three different typical analyses are shown with other color, and time 0 indicates initial time of internal actomyosin fraction effusion into external cytosolic extract.

## Chapter 3

## A Novel Mechanism of Sol – Gel Conversion in Amoeboid Locomotion

### 3-1 Abstract

Amoeboid locomotion is one of the typical modes of cell migration. During cell locomotion, cytoplasmic sol–gel conversion of an actomyosin system is thought to play an important role. However, the mechanisms underlying sol–gel conversion remain unclear. I used the experimental model system of bleb-driven amoeboid locomotion (IVA in Chapter 2) to elucidate the mechanisms of cytosolic sol-gel conversion. Rheological studies revealed that the actomyosin fraction exhibits shear thinning, indicating that the sol–gel state of actomyosin can be regulated by the shear rate. Furthermore, studies of the living cell indicated that the shear-shinning property is also well correlated with sol–gel conversion in the similar order of shear rate. These results suggest that the inherent sol–gel transition property plays an essential role in the self-regulation of autonomous translational motion in amoeba.

## 3-2 Introduction

Amoeba cytoplasm has sol and gel layers, and the sol layer is enclosed by the gel layer (Mast, 1923, 1926; Figure 1). During locomotion, the sol layer flows toward the direction of locomotion, while the gel layer is fixed. The sol in the anterior region is then transferred to the gel in parallel with cytoplasmic motion cessation and *vice versa* in posterior region. During amoeboid locomotion, cytoplasmic sol and gel states must be spatiotemporally regulated. If the cytoplasmic gel and sol configuration is uncontrolled, the cell cannot migrate in the desired direction. Although sol–gel conversion phenomena in amoeboid locomotion have been studied since the early 20th century (Mast, 1923; Mast, 1926), its mechanistic basis remains unclear, because of bleb-driven amoeboid locomotion complexity. It is generally believed that intracellular calcium ion concentration regulates cytoplasmic sol–gel conversion, because many actin binding proteins control sol-gel state of actin in a calcium dependent manner *in vitro* (Janson & Taylor, 1993). Generally, a high concentration of calcium ion induces solation, and a low concentration does gelation. Accordingly, calcium ion concentrations should be high in the sol region and low in the gel region of the cell. However, reports on calcium ion distribution in amoeba cells are conflicting. High calcium ion concentrations in posterior regions (Gollnick *et al.*, 1991; Kuroda *et al.*, 1998; Taylor *et al.*, 1980), in anterior regions (Taylor *et al.*, 1980), and low concentrations throughout the cell (Cobbold, 1980) have been reported. Hence, I become to think the presence of other calcium-independent mechanisms of cytoplasmic sol-gel conversion. As mentioned above in Chapter 2, I had developed a bleb-driven amoeboid locomotion model system, in which the amoeboid locomotion was

reconstituted with the cytoplasmic extract and the actomyosin fraction from *A. proteus* under defined calcium ion condition. In this Chapter, I describe a novel mechanism of the cytoplasmic sol-gel conversion using the model system.

### 3-3 Materials and Methods

#### Cell culture

Mass culture of *A. proteus* was performed as described previously (Nishihara *et al.*, 2008). In brief, *A. proteus* was cultured in the KCM medium (7 mg/l KCl, 8 mg/l $CaCl_2$, and 8 mg/l $MgSO_4 \cdot 7H_2O$) at 25°C and fed with *T. pyriformis*. Cells were starved for at least 2 days before use to avoid contamination with *T. pyriformis*.

#### Preparation of the IVA system

All preparations were at 2°C carried out, and movement was observed at room temperature. Ten grams of *A. proteus* was suspended in an EMP solution (2 mM EGTA, 2 mM $MgCl_2$, 20 mM PIPES-KOH, pH 7.0) and centrifuged at 6,000 × *g* for 2 min and after removed the supernatant. Then obtained precipitate was centrifuged at 600,000 × *g* for 20 min to obtain a cytoplasmic extract. The precipitate was suspended in a 3 M KCl solution (3 M KCl, 2 mM $MgCl_2$, 1 mM DTT, 20 µg/ml leupeptin, 20 µg/ml pepstatin A, 20 mM imidazole-HCl, pH 7.0) and centrifuged at 400,000 × *g* for 10 min. The resultant supernatant was dialyzed against 50 mM KCl, 2 mM EGTA, 2 mM $MgCl_2$, 1 mM DTT, 0.2 mM ATP, 20 mM imidazole-HCl, pH 7.0 for 5 h. Actomyosin was collected by centrifugation at 20,000 × *g* for 5 min and suspended in a 150 µl EMP buffer containing 1 mM DTT to prepare an actomyosin fraction. ATP at a final concentration of 2 mM was added to either the amoeba extract or the actomyosin fraction or both. Concentrations of proteins in both the fractions were determined by the method of Bradford with

bovine serum albumin as a standard, and the concentrations of both were approximately 20 mg/ml.

### Rheological studies

I processed a thin silicon sheet (SR-200, Tigars Polymer, Osaka, Japan) into a chamber (Figure 2) using a cutting machine (Craft ROBO pro, Graphtec, Kanagawa, Japan). I used a real-time confocal system (IX71, Olympus; CSU-X1, Yokogawa, Tokyo, Japan; iXon+, Andor, Belfast, UK) to obtain a fluorescence image of the actomyosin fraction containing fluorescent microspheres (FluoSpheres polystyrene microspheres 1 μm, Invitrogen). *A. proteus* was stained with MitoTracker Deep Red FM (Invitrogen) to observe cytoplasmic flow *in vivo*. Data analyses were performed using ImageJ and Igor 6.22A (WaveMetrics).

### Statistical analysis.

Statistical analysis was carried out using Igor 6.22A (WaveMetrics).

### 3-4 Results and Discussion

To simplify the flow of the model system, I made submillimeter silicon channel and observed flow patterns of the actomyosin fraction using fluorescent microsphere and real time confocal microscopy (see Material and Method for details). A flow chamber of silicone elastomer was immersed in the cytoplasmic extract, and the actomyosin fraction was injected into the chamber (Figure 2). Boundary surface between the actomyosin fraction body and external cytoplasmic extract was formed in trigonal space, and the narrow channel was filled with the actomyosin gel composed of the actomyosin fraction body. Movement of actomyosin fraction bulged as seen in the IVA system was observed in the trigonal space, and the actomyosin fraction in the narrow channel flowed toward the actomyosin body in the trigonal space. The actomyosin gel flow profiles in the narrow channel were examined using fluorescent microbeads for particle image velocimetry with real-time confocal microscopy.

Figure 3 and 4 show velocity distribution of fluorescent beads in four observations with different average velocities. In the slowest case (the maximum speed ≃ 41 μm/s), the distribution of velocities of individual fluorescent microspheres exhibited the Hagen-Poiseuille flow profile (Figure 4, bottom shown in green). In the other cases with higher average velocities, the distribution was split into two plateaus by emergence of slipping interfaces. It is evident in the histograms of velocities because there are two velocity peaks, one corresponding to behavior of microspheres near the channel wall and the other to that of microspheres in the central part of the channel (Figure. 3). In the split flow profiles, inner and outer flows can be fitted by $-d^2$ lines ($d$ is displacement from the center of the channel),

so that each of flows performed the Hagen-Poiseuille flow. Because myosin thick filaments possess many bipolar actin-binding sites, actin and myosin filaments continually disassociate and associate each other in the presence of ATP (Toyota *et al.*, 2011). This dissociation and association allow reformation of the gel network under low shear condition. Therefore, the actomyosin keeps its gel state while it may exhibit some fluidic behavior under a low shear rate in the presence of ATP. In contrast, under fast flow or high shear rate, the connections between actin and myosin are broken by shear stress. Once the network broke, a percolation network of the actomyosin gel did not emerge during the motion (Figure. 4). In fast flow or under a large shear stress, the stress produces a slipping plane where connection between actin and myosin are continuously broken by the shear stress, while the other parts of the cytoplasm are still in the gel phase. This slipping plane formation began at approximately 0.5 $s^{-1}$ of shear strain and was maintained in regions with higher rates (2–4 $s^{-1}$). To examine velocities of cytoplasmic flow in living cell, *A. proteus* were stained by MitoTracker, and velocities of mitochondria were measured (Figure 6). In this analysis, a slipping plane formed above approximately 0.25 $s^{-1}$ of shear strain and the shear strain around the slipping plane was approximately 2 $s^{-1}$.

Cytoplasmic sol–gel conversion is important in amoeboid locomotion (Mast, 1923, 1926; Figure 1). When the elastic structure inside a cell cannot withstand pressure from the active cortex, the entire cytoplasm is spontaneously carried into a new pseudopod. On the other hand, a cell whose entire cytoplasm becomes a rigid gel state could not migrate. Accordingly, cytoplasmic sol and gel states must be regulated spatiotemporally depending on intra- and extracellular environments. In this situation, the mechanism of sol–gel transition corresponding to shear strain

would be useful in regulating the cell migration. Using such property, amoeba could be free from complex regulation. Although several studies were reported supporting my study (Kunita *et al.*, 2012; Marion *et al.*, 2005; Rogers *et al.*, 2008), the importance of cytoplasmic sol–gel conversion that induced by shear stress in the regulation of cellular processes has not been recognized.

Intracellular calcium ion concentration is, indeed, one of the critical factors for cytoplasmic sol–gel conversion (Janson & Taylor, 1993). A high concentration of calcium ion induces a sol state through actin binding protein and a low concentration does a gel state. If calcium ion concentration is the only determinant of the sol-gel conversion, it should be high in the sol region and low in the gel region of the cell. However, reports on calcium ion distribution in the amoeba cell are conflicting. Some reports argue high calcium ion concentrations in posterior regions (Gollnick *et al.*, 1991; Kuroda *et al.*, 1998; Taylor *et al.*, 1980a), some do high calcium in anterior regions (Taylor *et al.*, 1980a), and while others do low concentrations throughout the cell (Cobbold, 1980). There may be a possibility that some of the conflicting reports have some technical problems for estimation of calcium ion concentration, but it may be true that sol-gel states in the cytoplasm is not determined solely by calcium. If so, sol-gel conversion under different calcium condition can be partly explained by my hypothesis of mechanically responsive sol–gel transition, at least in amoeboid migration. The cytoplasm with an intrinsic nature of mechanically responsive sol–gel conversion can behave as an elastic gel under static conditions. On the other hand, rupture of the static balance by contraction of a part of cell cortex will cause dynamic protrusive excursion through a mechanical gel-to-sol transition of a central part of the cytoplasm, as observed in my

model system. Calcium ion would be a constitutive trigger or regulator for the cortex organization, affecting strength, thickness, or activity of cytoplasm to breaking the static balance of the amoeba cell, and such effects of calcium may determine direction of cytoplasmic flow, that is, direction of migration.

Thus, I have provided a new insight into cytosolic sol–gel conversion mechanism, in which an active actomyosin cortex system exhibits mechanically responsive viscoelasticity. This physical property is thought to be sufficient to explain cytosolic sol–gel conversion during amoeboid locomotion. Although almost all my results were observed in *in vitro* systems, they suggest that organisms generally use this unique physical property of the active actomyosin for driving amoeboid movement.

### 3-5 Figures

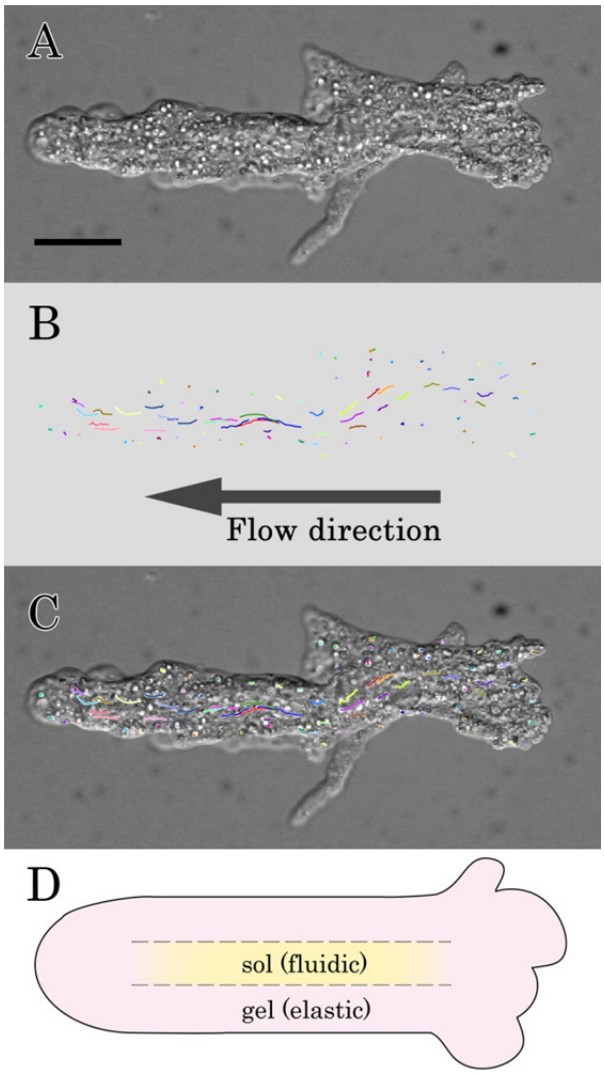


**Figure 1. Cytoplasmic distribution of sol and gel in amoeba cell.** (A) An bright field image of a locomoting amoeba. Trajectories of cytoplasmic particle flow during 1 s duration are shown in (B). (C) is a merged image of (A) and (B). A scheme for the distribution of cytoplasmic sol and gel is shown in (D). Amoeba cytoplasm has two layers of sol and gel, in which the sol layer is enclosed by the gel layer. Scale bar, 50 μm.

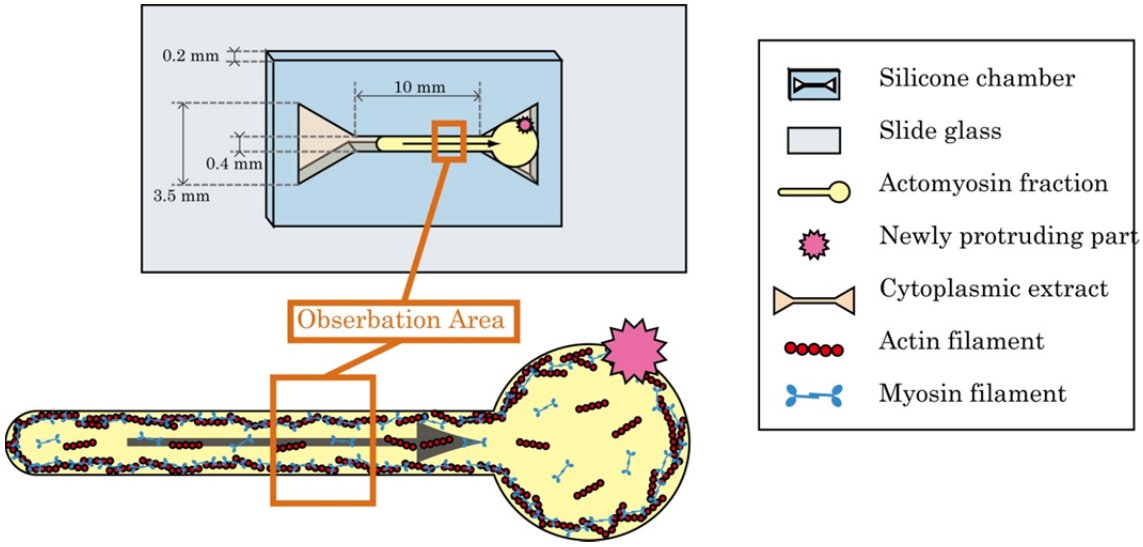


**Figure 2. A schematic diagram of rheological analysis in the IVA system.** To make a chamber, a silicon sheet with 0.2 mm thick was cut as in panel. The cut silicon sheet was contacted with a siliconized slide glass, and the chamber was immersed in the cytoplasmic extract. After covering the narrow rectangular space with siliconized cover slip, the actomyosin fraction was injected into a rectangular space of the chamber. A shape of the injected actomyosin fraction is represented as yellow. I observed a part of narrow rectangular space (orange) with real-time confocal microscope.

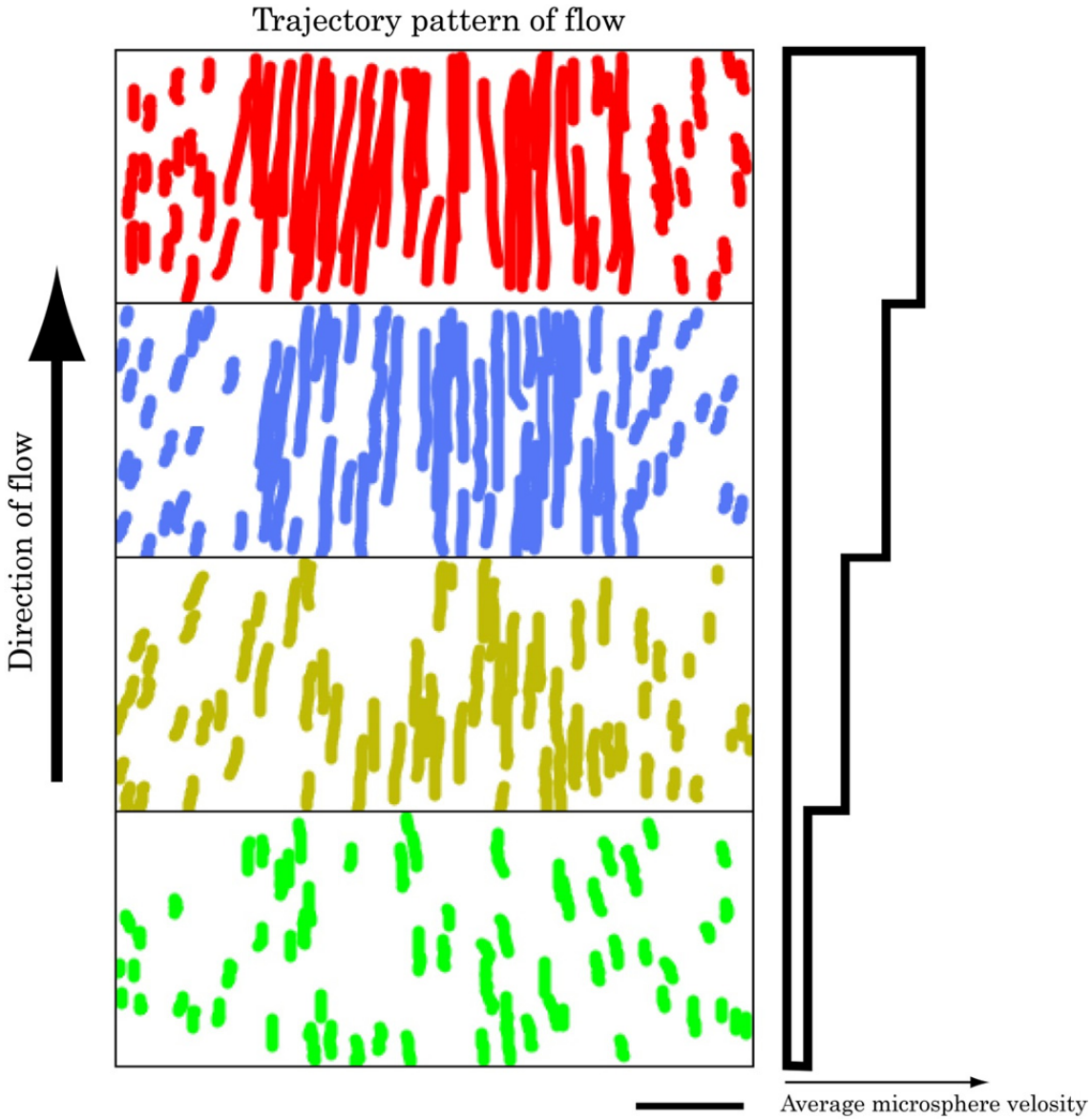


**Figure 3. Trajectory of individual microspheres movement in rheological analysis.**

The actomyosin fraction flow profiles in the narrow channel were examined using fluorescent microspheres. The typical trajectory of individual microspheres movement for 0.3 sec with four different average velocity are represented, and colors reflect difference of average microsphere velocity.

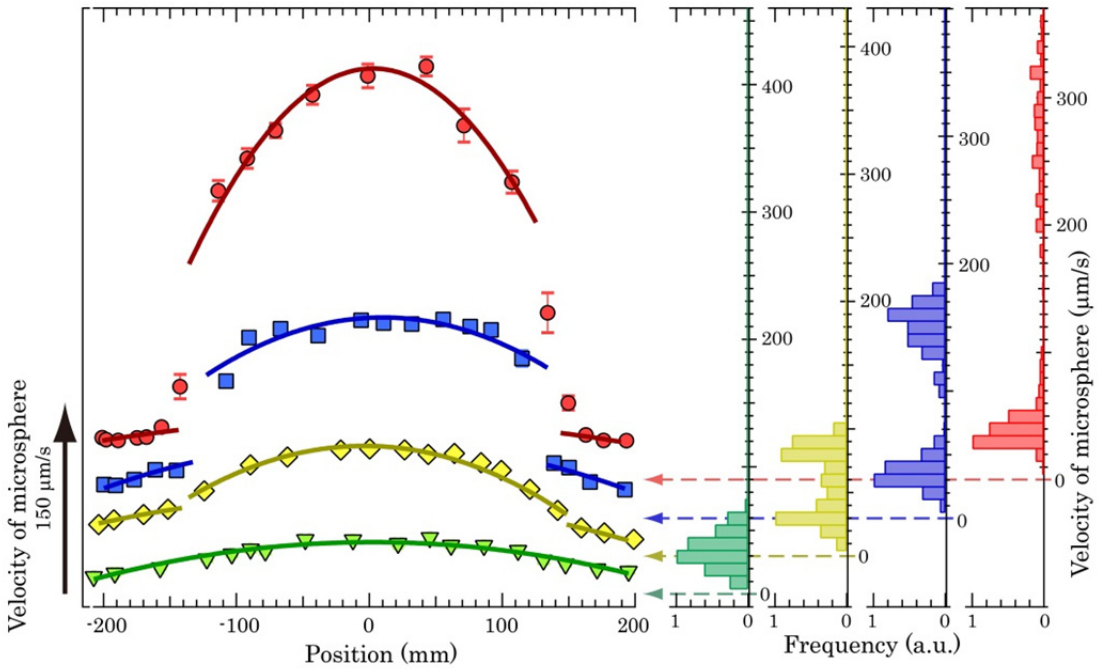


**Figure 4. Rheological characterization of cytoplasmic flow in a narrow chamber with the IVA system.** The typical observation of cytoplasmic flow with four different average velocities of microspheres in Figure 3 are analyzed, and shown as a plot of particle velocities against distance from the center of the chamber. Distribution of particle velocities is also shown as histograms in the right. Colors used to indicate data are the same as used in Figure 3. Error bars show s.e.m. (n=25 at each point).

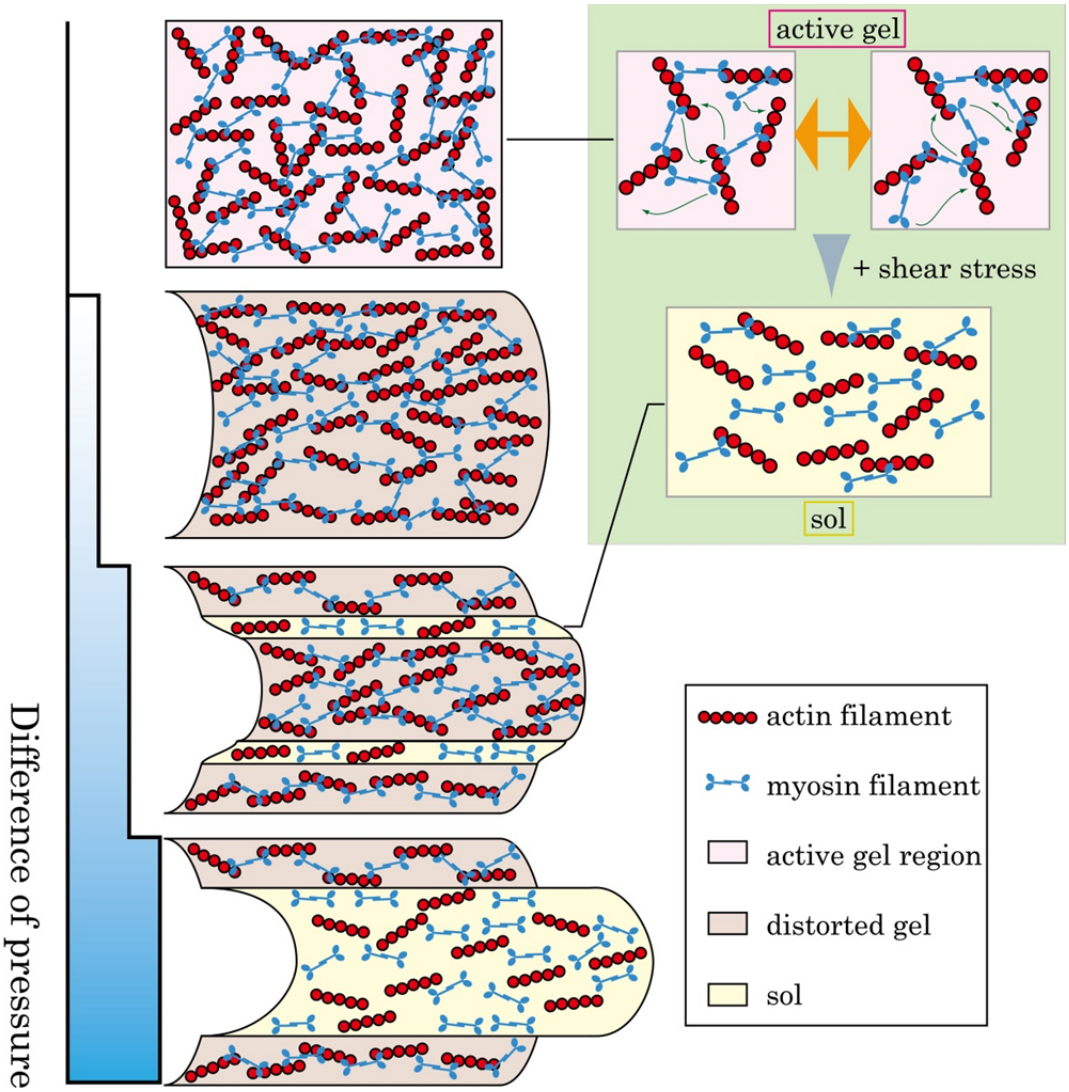


**Figure 5. A proposed mechanism of cytosolic sol–gel conversion.** Since actin and myosin filaments repeatedly bind and release each other in the presence of ATP (right, upper panel), an actomyosin dispersed in water behaves as an active gel, in which the actomyosin gel may have some fluidic characteristics under a small shear stress (left, 2nd panel). In contrast, in fast flow or under a large shear stress, the stress produces a slipping plane where connection between actin and myosin are continuously broken by the shear stress, while the other parts of the cytoplasm are

still in the gel phase (left, 3rd panel). If the shear stress becomes large, the whole center part of the cytoplasm is converted into the sol phase (left, bottom panel).

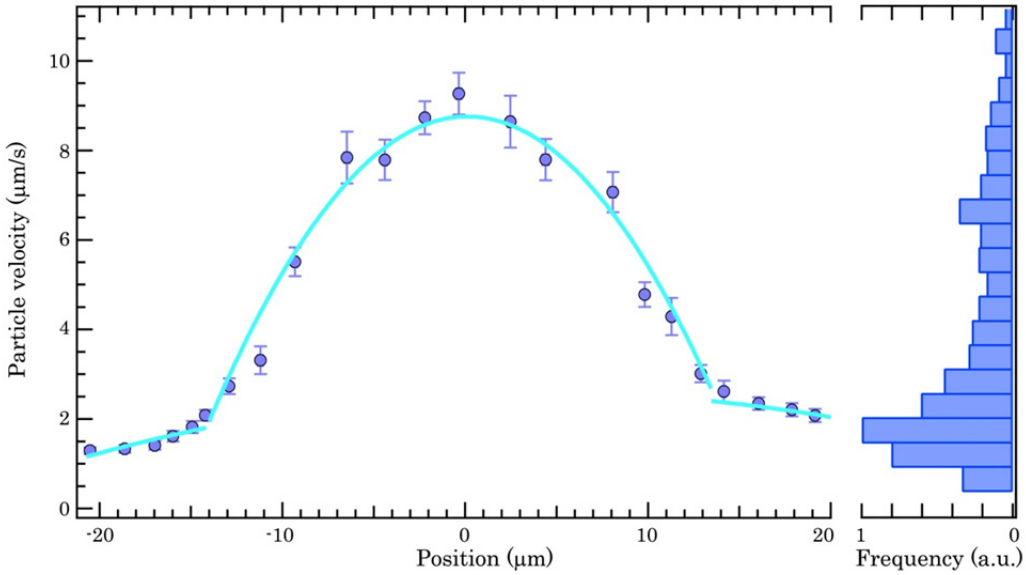


**Figure 6. Rheological characterization of cytoplasmic flow monitored by mitochondrial migrations in the living amoeba.** A profile of particle movement in a living amoeba was examined by monitoring movement of fluorescently-labeled mitochondria. Velocities of indivisual mitochondoria in the cytoplasmic flow are shown as in figure4. Error bars show s.e.m. (n=20 at each point).

## Chapter 4 Effects of Calcium Ion on Amoeboid Motion in the Model System and the Living Cell


### Abstract 4-1

To assess the role of calcium ion in cell locomotion, I evaluated the effect of calcium ion on the IVA system. A [$Ca^{2+}$] in actomyosin fraction was not important in activity of IVA system. On the other hand, that in the cytoplasmic extract prominently influenced the movement activity of the IVA system. A high [$Ca^{2+}$] promoted formation of pseudopod-like structure while a low [$Ca^{2+}$] inhibited such movement. To examine whether the same event was observed *in vivo*, I performed calcium imaging studies. Increasing of [$Ca^{2+}$] was observed in the anterior region of moving amoeba cells. In addition, a pseudopod could be induced artificially in *A. proteus* that expressed channel-rhodopsin-2, a light-gated cation-selective channel. From these observations, I concluded that the elevation of [$Ca^{2+}$] induces pseudopod formation in living cells.

## 4-2 Introduction

Actomyosin contraction at cell cortex produces a motive force for amoeboid locomotion in a giant free-living amoeba, *A. proteus* (Chapter 2; Goldacre & Lorch, 1950; Goldacre, 1956, 1961, 1964; Jahn, 1964; Kawakatsu *et al.*, 2000; Marsland, 1956; Mast, 1923, 1926; Oh & Jeon, 1998; Rinaldi & Jahn, 1963; Rinaldi *et al.*, 1975; Stockem *et al.*, 1982, 1984; Taylor *et al.*, 1980b; Yanai *et al.*, 1996). This type of locomotion is called bleb-driven amoeboid locomotion (Charras, 2008; Fackler & Grosse, 2008). During the locomotion, actin and myosin play an important role, and their activities are regulated by calcium ion (Chapter 3; Cobbold, 1980; Gollnick *et al.*, 1991; Kuroda & Sonobe, 1981; Kuroda *et al.*, 1998; Taylor *et al.*, 1980a). During amoeboid locomotion, the cytoplasm of *A. proteus* exhibits active sol-gel conversion (Chapter 3), which is controlled by actin-binding proteins and calcium ions; a high concentration of calcium ion generally induces a sol state and a low concentration induces a gel state (Janson & Taylor, 1993). Although concentrations of cytoplasmic calcium were measured in several experiments, reports on the distribution of calcium ions in amoeba cells are conflicting (Cobbold, 1980; Gollnick *et al.*, 1991; Kuroda *et al.*, 1998; Taylor *et al.*, 1980a). Some reported high calcium ion concentrations in posterior regions (Gollnick *et al.*, 1991; Kuroda *et al.*, 1998; Taylor *et al.*, 1980a), some did in anterior regions (Taylor *et al.*, 1980a), and others reported low concentrations throughout the cell (Cobbold, 1980). In Chapter 3, I proposed that a part of this mystery could be explained by the hypothesis of mechanically responsive sol–gel transition. If this is true, a function of calcium ion is still unclear. To clarify this point, I tried to examine effects of calcium ion on movement in the IVA system and *in vivo*. First, I checked an influence of $[Ca^{2+}]$ on the activity of the

IVA system. To investigate the role of calcium ion *in vivo*, I performed calcium ion imaging in living cell using Furo4 and FraRed, which are fluorescent calcium ion indicators, and tried to induce pseudopod formation in cells which expressed a photo-activatable cation channel, channel-rhodopsin-2 (Nagel *et al.*, 2003).

4-3 Materials and Methods

## Cell culture

Mass culture of *A. proteus* was performed as described previously (Nishihara *et al.*, 2008). In brief, *A. proteus* was cultured in the KCM medium (7 mg/l KCl, 8 mg/l $CaCl_2$, and 8 mg/l $MgSO_4 \cdot 7H_2O$) at 25°C and fed with *T. pyriformis*. Cells were starved for at least 2 days before use to avoid contamination with *T. pyriformis*.

## Preparation of the IVA system

All preparations were at 2°C carried out, and movement was observed at room temperature. Ten grams of *A. proteus* was suspended in an EMP solution (5 mM EGTA, 6 mM $MgCl_2$, 30 mM PIPES-KOH, pH 7.0) and centrifuged at 6,000 × *g* for 2 min and after removed the supernatant. Then obtained precipitate was centrifuged at 600,000 × *g* for 20 min to obtain a cytoplasmic extract. The precipitate was suspended in a 3 M KCl solution (3 M KCl, 2 mM $MgCl_2$, 1 mM DTT, 20 µg/ml leupeptin, 20 µg/ml pepstatin A, 20 mM imidazole-HCl, pH 7.0) and centrifuged at 400,000 × *g* for 10 min. The resultant supernatant was dialyzed against 50 mM KCl, 2 mM EGTA, 2 mM $MgCl_2$, 1 mM DTT, 0.2 mM ATP, 20 mM imidazole-HCl, pH 7.0 for 5 h. Actomyosin was collected by centrifugation at 20,000 × *g* for 5 min and suspended in a 150 µl EMP buffer containing 1 mM DTT to prepare an actomyosin fraction. ATP at a final concentration of 1 mM was added to the cytoplasmic extract and/or the actomyosin fraction. Concentrations of proteins in both fractions were determined by the method of Bradford with bovine serum albumin as a standard. The concentrations of both were approximately 20 mg/ml.

**Treatment of the IVA system with various concentrations of calcium ion.**

To control [$Ca^{2+}$] in the cytoplasmic extract, ten times as high concentration as EMP solution (10 x EMP solution) was used. $CaCl_2$ was added to the 10 x EMP solution to adjust [$Ca^{2+}$], and free [$Ca^{2+}$] was calculated from the dissociation constants by using the computer analysis program (Kohno and Shimmen, 1988). The pH of the 10 x EMP solution containing various [$Ca^{2+}$] was finally adjusted to 7.0 with KOH. To prepare [$Ca^{2+}$] controlled cytoplasmic extract, a one tenth volume of the 10 x EMP was added to the cytoplasmic extract. On the other hand, to prepare [$Ca^{2+}$] controlled actomyosin fraction, the actomyosin fraction was centrifuged at 20,000 × *g* for 10 min and resuspended in a [$Ca^{2+}$] controlled EMP solution containing 1 mM DTT. ATP at a final concentration of 1 mM was added to either the [$Ca^{2+}$] controlled cytoplasmic extract or the [$Ca^{2+}$] controlled actomyosin fraction. Concentrations of proteins in both the fractions were determined by the method of Bradford with bovine serum albumin as a standard, and the concentrations of both were approximately 20 mg/ml. One microliter of the [$Ca^{2+}$] controlled actomyosin fraction was injected into 10 µl of the [$Ca^{2+}$] controlled cytosolic extract on a cover glass. Movement was observed by a stereomicroscopy (SZH, Olympus) with dark-field illumination and recorded by a CCD camera (KY-F550, Victor).

**Measurement of viscosity of the cytoplasmic extract.**

Viscosity assay was performed as described in the previous study (MacLean-Fletcher & Pollard, 1980). In brief, cytoplasmic extract was mixed with

10 x EMP solution on ice, injected into capillary tubes, and then warmed to 25°C. After 5 min, an iron boll with 1 mm diameter falled into the capillary to measure the apparent viscosity. The condition where this experiment was performed is essentially the same as those for the IVA movement assay in Figure 2. Statistical analysis was carried out using Igor 6.22A (WaveMetrics).

**Measurement of intercellular calcium ion concentration**

To measure [$Ca^{2+}$] *in vivo*, 0.2 mM Fluo4 (Invitrogen) and 0.8 mM FuraRed (Invitrogen) were microinjected into *A. proteus*. Fluorescent time-laps images were obtained by a confocal fluorescence microscope (Axioplan 2 and LSM510, Carl Zeiss, Oberkochen, Germany). The ratio images were calculated using R (a language and environment for statistical computing and graphics).

**Artificial pseudopod formation assay with channel-rhodopsin-2 expressing amoeba**

A plasmid of channel-rhodopsin-2 tagged with EYFP was gifted from Prof. K. Hatta (University of Hyogo, Hyogo, Japan). The mRNA was prepared using *in vitro* transcription kit (mMESSAGE SP6 Kit, Life Technologies, Carlsbad, CA, USA). Prepared mRNA (2 μg/μl in water) were microinjected into *A. proteus*. After 30 min, cells with fluorescence were collected and used to perform analyses. The collected cells were suspended in KCM medium or KM medium (7 mg/l KCl and 8 mg/l $MgSO_4 \cdot 7H_2O$). To avoid light damage, cells were observed by green light, and partially irradiated by blue light using a fluorescent microscope with narrow slit (Axioplan, Carl Zeiss). The times of irradiation were one second in all experiments.

## 4-4 Results and Discussion

To assess the role of the calcium ion in the motile activity of the IVA system, the concentrations of calcium ion was controlled by the $Ca^{2+}$-EGTA buffer system (see Materials and Methods for details) and movements of the IVA system were observed (Figure 1). When panels in the same column in Figure 1 are compared, it is evident that the concentrations of calcium ion in the actomyosin fraction do not influence activity of the IVA system. On the other hand, the activity of the IVA system was strongly influenced by the concentration of calcium ion in cytoplasmic extract (*cf.* panels in the same row in Figure 1). When the concentrations of calcium ion in the cytoplasmic extract were in the range from $1.0\times10^{-8}$ M to $1.0\times10^{-6}$ M, the IVA system did not move. In contrast, when those were from $4.0\times10^{-6}$ M to $1.0\times10^{-4}$ M, actomyosin fraction moved like amoeba. Those observations indicate that the concentrations of calcium ion in the cytoplasmic extract are important in activity of the IVA system, and calcium ion promotes making pseudopod-like structures. Previous reports demonstrated that cytoplasmic extract gelled in low concentration of calcium, and sled in its high concentrations (Janson & Taylor, 1993). To determine the relation between cytoplasmic sol-gel state and activity of the IVA system, I measured viscosity of the cytoplasmic extract with variety concentrations of calcium ion. I also measured the activity of the IVA system prepared with same conditions. The results showed that the cytoplasmic extract became gel at $[Ca^{2+}] \leq 1.0 \times 10^{-6}$ M, and the motility of the actomyosin fraction was lost at the same range of $[Ca^{2+}]$, suggesting that gelation of the cytoplasmic extract inhibits the motility of the IVA system (Figure 2). In the gelled cytoplasmic extract, actin must form a strong network, so actomyosin in the boundary surface could not contract. Thus, I

predicted that before a pseudopod was formed, the concentration of calcium ion was increased in a prospective region of pseudopod formation *in vivo*. However, reports on calcium ion distribution in cells are conflicting. As mentioned in Chapter 3, different parts of an amoeba cell were reported to have high calcium ion concentrations (Cobbold, 1980; Gollnick *et al.*, 1991; Kuroda *et al.*, 1998; Taylor *et al.*, 1980a). These studies used aequorin or fura-2 as calcium indicators. The excitation wavelength of fura-2 is in ultraviolet region, which has harmful effects on *A. proteus*. These effects may cause above-mentioned conflicts. Therefore, I measured intercellular concentration of calcium ion using Fluo-4 and FuraRed, the excitation wavelengths of these indicators are in a blue region. As a result, the increase of calcium-ion concentration was observed in both anterior (Figure 3) and posterior regions (data not shown). These results were similar to previous report in which aequorin was used (Taylor *et al.* 1980a). The increase of calcium ion in the posterior region might contribute to cytoplasmic solation (discussed in Kuroda *et al.* 1998). In the anterior region, after increase of the calcium ion concentration, a pseudopod was elongated. Therefore, the elevation of calcium-ion concentration may be a trigger of pseudopod formation. To further investigate this possibility, channel-rhodopsin-2, which is a cation-selective channel that that gated by blue-light (Nagel *et al.* 2003), was expressed in *A. proteus*, and morphological change after irradiating a part of the cell with blue light was monitored by time-lapse imaging. In the irradiated region, a pseudopod was formed after a few seconds (Figure 4). Such irradiated light-depend pseudopod formation was never observed in amoeba cells that did not express channel-rhodoprin-2 (Figure 2A). When calcium ion was not added in the culture medium, new pseudopod formation

was not observed (Figure 5). From these observations, I conclude that the influx of extracellular calcium induces pseudopod formation. In *A. proteus*, actin filaments are bound to the plasma membrane in a calcium-dependent manner (Kawakatsu *et al.*, 2000). It is likely that calcium ion influx induces dissociation of actin from the cell membrane, and the cytoplasm is flowed into this fragile region. Therefore, calcium ion is supposed to have a pivotal role in determining the place of pseudopod formation. In this *in vivo* process, relationship between calcium induced solation and formation of a new pseudopod is still unclear. At least, in the IVA system, solation of the cytoplasmic extract induced by calcium ion contributes to form a new pseudopod-like structure. When the cytoplasm flows into the anterior region, shear force is produced to induce mechanical solation of the cytoplasm in this region (see chapter 2). This may cause flow of the cytosol into an area for potential pseudopod formation without any strict regulation of sol-gel conversion depended on calcium ion. Thus, once calcium ion flows into an amoeba cell, the intracellular auto-regulated system should work, and amoeba moves actively.

## 4-5 Figures

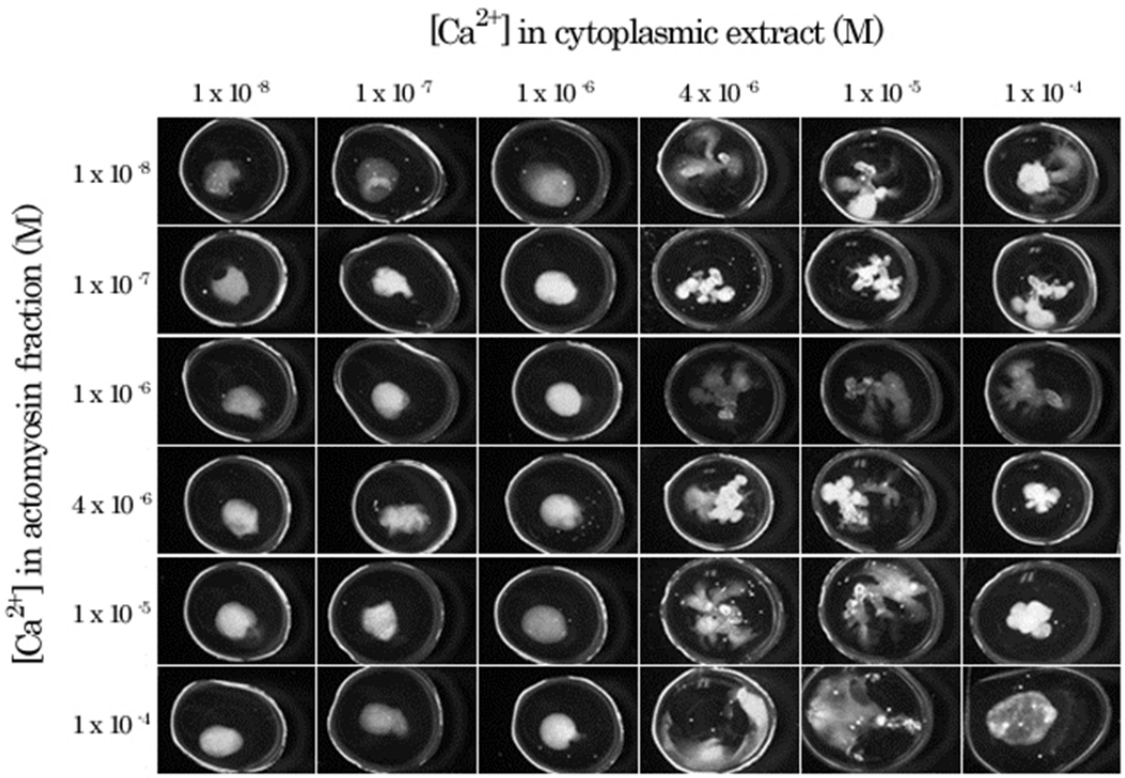


**Figure 1. The movement patterns of the IVA system in various combination of [$Ca^{2+}$].**

$Ca^{2+}$ concentrations in the cytoplasmic extract and that in actomyosin fraction were controlled by the $Ca^{2+}$-EGTA buffer in a range from $1.0\times10^{-8}$ M to $1.0\times10^{-4}$ M. [$Ca^{2+}$] in cytoplasmic extract and actomyosin fraction shown on the top and left, respectively. After 1 min incubation, shape of the actomyosin fraction was photographed.

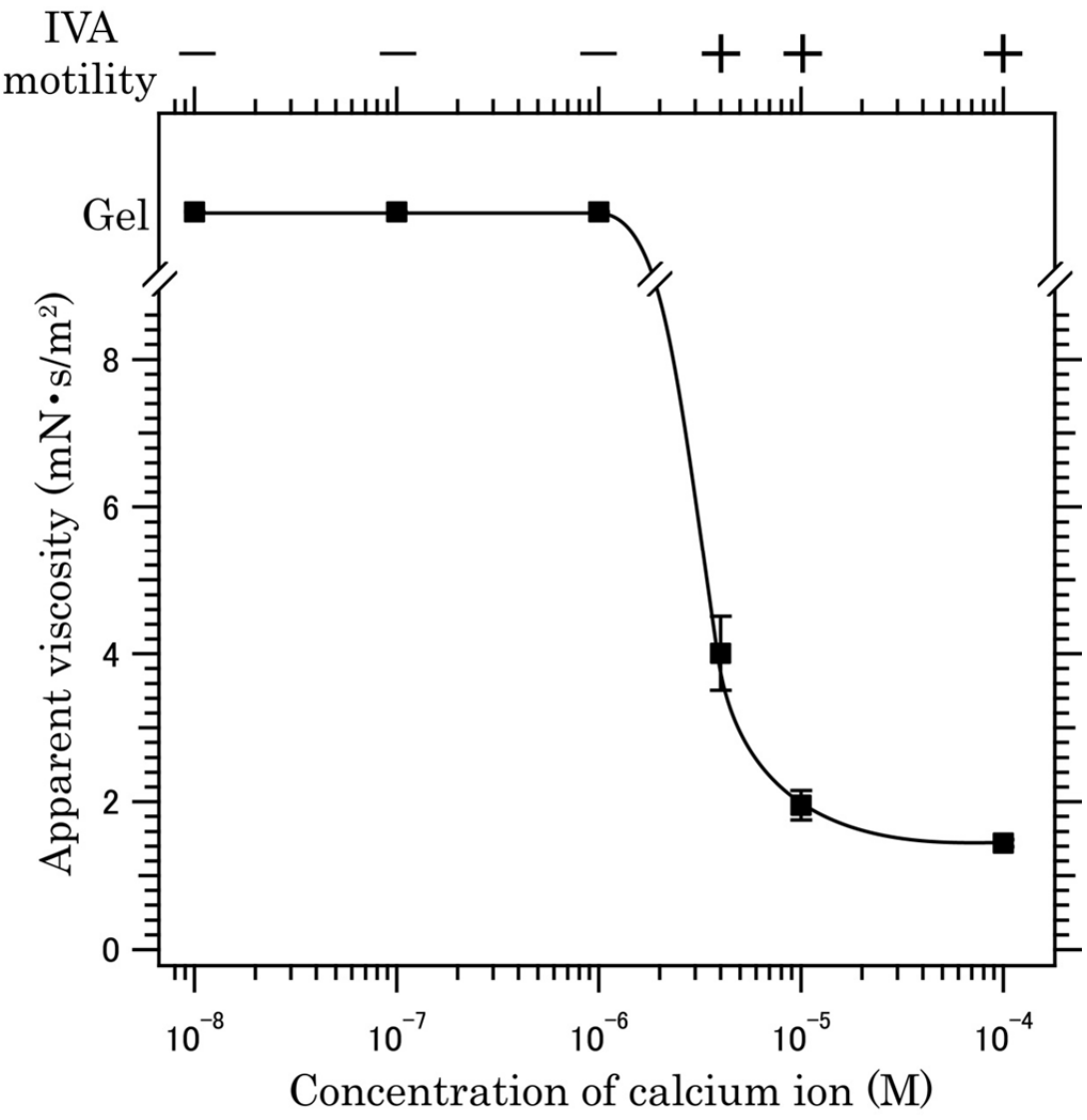


**Figure 2. Rheological characterization and motility at different [$Ca^{2+}$] in the cytoplasmic extract.** Apparent viscosity of the cytoplasmic extract at various [$Ca^{2+}$] was measured as described in Materials and Methods. Error bars show s.e.m. (n=5 at each point). Under the same condition, amoeboid movement of the IVA system was monitored, and the results were indicated as + or –on the top of the graph. Positions of the +/– marks represent [$Ca^{2+}$] used in the IVA system.

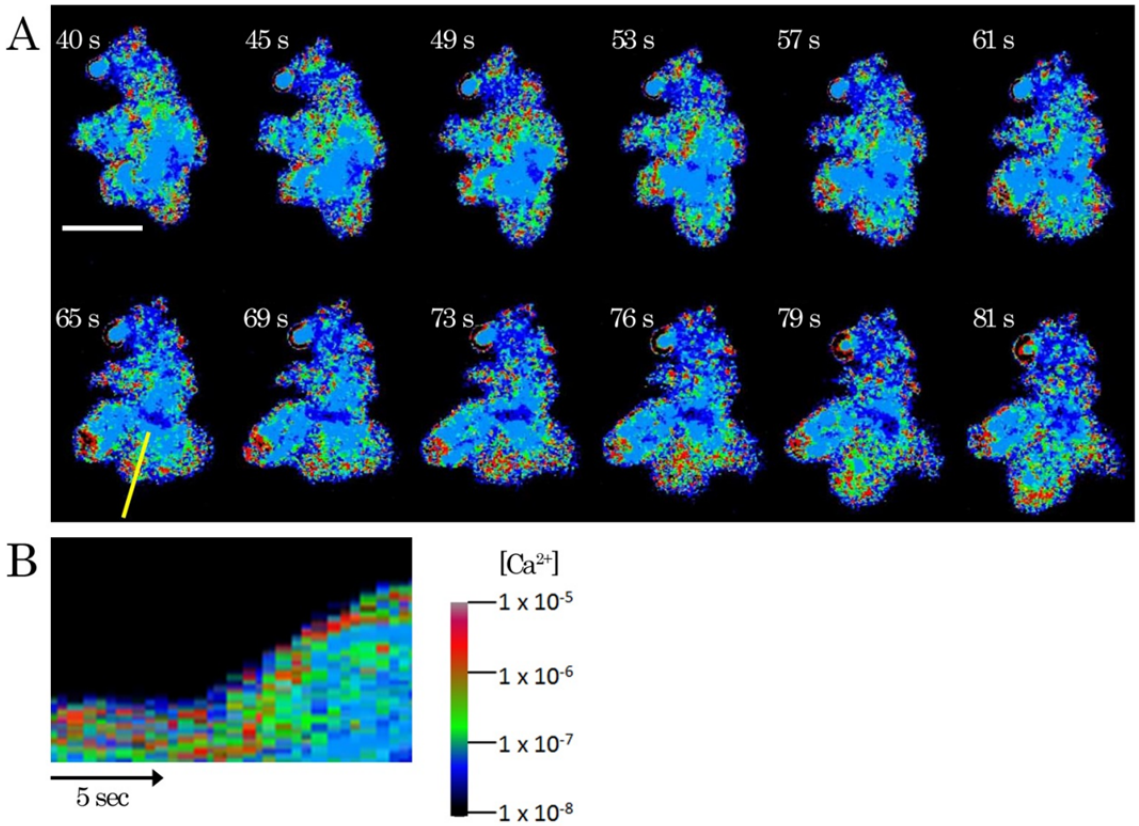


**Figure 3. Imaging of calcium concentration in living cell.** (A) Time-laps images of an *A. proteus* stained with fluorescent calcium indicators was shown. Upper-left numbers represent time points when the images were taken. (B) A kymograph of a part of the amoeba indicated with a yellow line in the panel (A). The results were shown form 65 s to 81 s. As shown in 76 s ~ 81 s panels in (A), this part formed a new pseudopod. An indicator for pseudo color expressed of $[Ca^{2+}]$ is shown in the center bottom part of the figure. Scale bar, 100 μm.

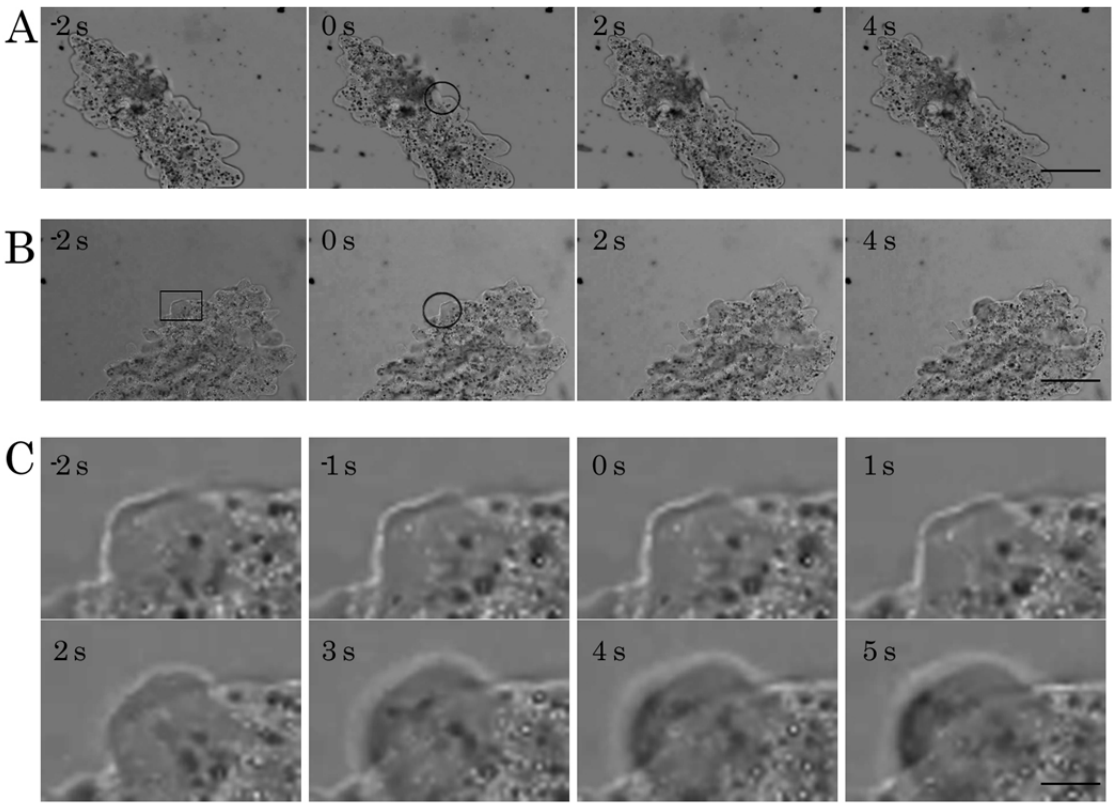


**Figure 4. Blue-light induced pseudopod formation in a living cell expressed channel-rhodopsin-2.** Amoeba cell wxpressing channel-rhodoprin-2 (B) and control cell (A) were cultured in KCM medium, and parts of these cells were irradiated with blue-light (circular areas) at time 0 sec. Scale bar, 100 μm. (C) a region specified with a rectangular in (B) was shown at higher magnification with 1 sec interval. Scale bar, 25 μm.

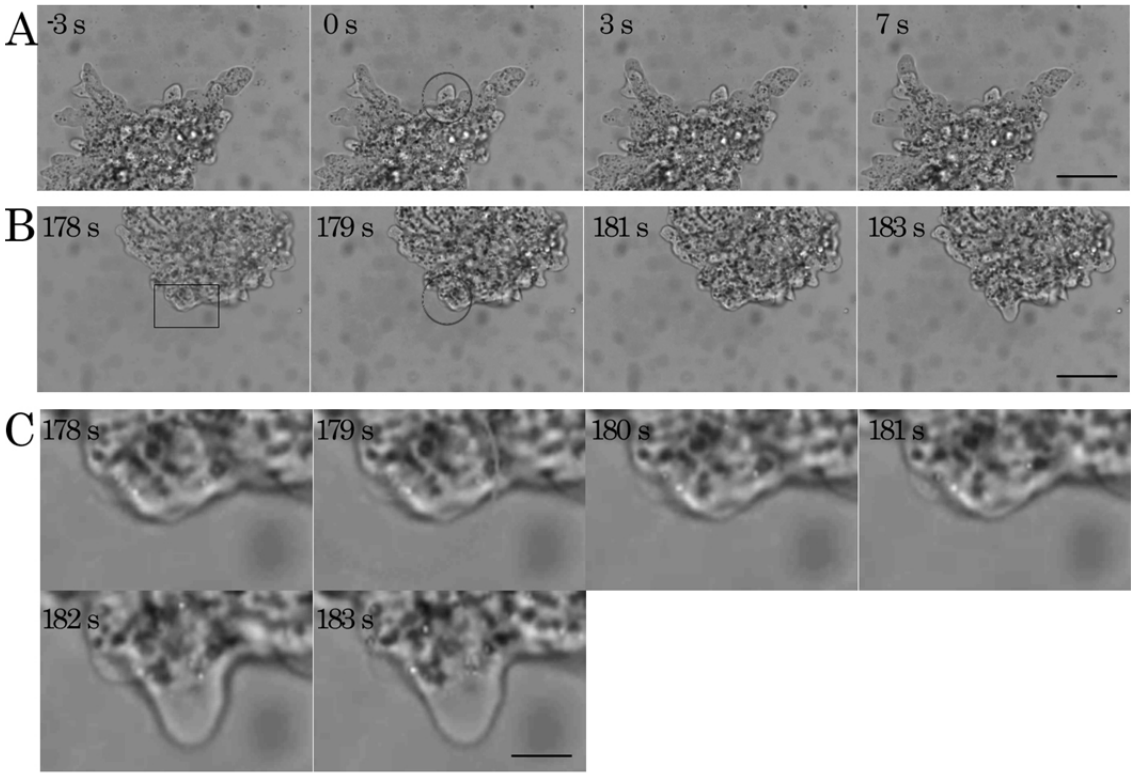


**Figure 5. Blue-light induced pseudopod formation in living cells expressing channel-rhodopsin-2 in the absence of extracellular calcium.** (A) Irradiation of a cell expressing channel-rhodprin-2 with blue light (circular areas) at time 0 sec was performed in the absence of extracellular calcium. Scale bar, 100 μm. (B) The same cell in (A) was irradiated with blue light at 179 sec in the presence of extracellular calcium. Bar = 100 μm. (C) A region specified with a rectangular in (B) was shown. Scale bar, 25 μm.

## Chapter 5 An Attempt to Make an Additional Model System, Which Is Enclosed by a Membrane

### 5-1 Abstract

To make another novel model system, I sought to enclose the IVA system with the membrane using cell-sized water droplets (CWD) surrounded by a single layer of phospholipids in mineral oil. When general phospholipids were used, actin was dispersed in droplets. However, positive charged amphiphile substituted for phospholipid allows me to obtain droplets in which actin filaments were accumulated beneath the droplet surface. Introduction of actomyosin fraction to these droplets, resulting the contraction of droplet surface. Since surface contraction is important process in generation of motive force in blebbing cells, this novel system is expected to be a model system to elucidate the mechanism of bleb-driven amoeboid locomotion.

## 5-2 Introduction

In bleb-driven amoeboid locomotion, the cell membrane plays important roles, especially, in definition of direction of movement (Charras, 2008; Fackler & Grosse, 2008). Partial detachment of the actin cortex from the cell membrane induces blebbig (Chapter 4; Blaser *et al.*, 2006; Keller *et al.*, 2002). Although my model system is excellent in tractable, changeable components arbitrarily and so on (see previous Chapters), it is not enclosed by a membrane (see Chapter 2). To make a model system more resembling to real amoeba, I sought to enclose the model system with a membrane. In this study, cell-sized water droplets with a lipid monolayer (CWD) were used. In comparison with the liposome system, the CWD is incomplete in some way. However, this system is easier to make than the liposome system, and the water phase of CWD can be used a model of the cytoplasm because the head group of a lipid at the water-oil interface faces the water phase (Hase &Yoshikawa, 2006). In bleb-driven amoeboid locomotion, accumulation of actin at the cell cortex is important in generation of motive force (Charras, 2008; Fackler & Grosse, 2008). As the first step, I sought to reconstitute this accumulation of actin using CWD.

## 5-3 Materials and Methods

### Cell culture

Mass culture of *A. proteus* was performed as described previously (Nishihara *et al.*, 2008). In brief, *A. proteus* was cultured in the KCM medium (7 mg/l KCl, 8 mg/l $CaCl_2$, and 8 mg/l $MgSO_4 \cdot 7H_2O$) at 25°C and fed with *T. pyriformis*. Cells were starved for at least 2 days before use to avoid contamination with *T. pyriformis*.

### Preparation of cytoplasmic extract and actomyosin fraction

All preparations were at 2°C carried out, and movement at room temperature was observed. Ten grams of *A. proteus* was suspended in an EMP solution (5 mM EGTA, 6 mM $MgCl_2$, 30 mM PIPES-KOH, pH 7.0) and centrifuged at 6,000 × *g* for 2 min and after removed the supernatant. Then obtained precipitate was centrifuged at 600,000 × *g* for 20 min to obtain a cytoplasmic extract. The precipitate was suspended in a 3 M KCl solution (3 M KCl, 2 mM $MgCl_2$, 1 mM DTT, 20 µg/ml leupeptin, 20 µg/ml pepstatin A, 20 mM imidazole-HCl, pH 7.0) and centrifuged at 400,000 × *g* for 10 min. The resultant supernatant was dialyzed against 50 mM KCl, 2 mM EGTA, 2 mM $MgCl_2$, 1 mM DTT, 0.2 mM ATP, 20 mM imidazole-HCl, pH 7.0 for 5 h. Actomyosin was collected by centrifugation at 20,000 × *g* for 5 min and suspended in 150 µl of EMP buffer containing 1 mM DTT to prepare an actomyosin fraction. ATP at a final concentration of 2 mM was added to either the amoeba extract or the actomyosin fraction or both. Concentrations of proteins in both the fractions were determined by the method of Bradford with bovine serum albumin as a standard, and the concentrations of both were

approximately 20 mg/ml. To make a diluted cytoplasmic extract, the cytoplasmic extract was diluted by CEMP solution (4.72 mM $CaCl_2$, 5 mM EGTA, 6 mM $MgCl_2$, 30 mM PIPES-KOH, pH 7.0), in which the concentration of calcium ion was $1 \times 10^{-5}$ M. To observe actin, rhodamine phalloidin (Invitrogen) at final concentration of 7 nM was added to the (diluted) cytoplasmic extract, and mixture of cytoplasmic extract and actomyosin fraction.

### Making and observation of CWD

The CWD was prepared as described previously (Kato *et al.*, 2009). In brief, The amphiphile, 1,2-dioleoyl-3-trimethylammonium-propane chloride (DOTAP), were dissolved in chloroform to be 10 mM. The DOTAP solution was dried in a nitrogen stream and allowed to settle under vacuum overnight. Mineral oil was added to the dried films to be 1 mM of DOTAP, and sonicated at 60 °C for 90 min, which resulted in dispersed DOTAP in oil. Finally, to obtain CWD, 5–10 % (vol/vol) of either the diluted cytoplasmic extract, the cytoplasmic extract or the mixture of cytoplasmic extract and actomyosin fraction was added to the lipids in the oil solution, and emulsification was performed by pipetting. Obtained droplets were observed using a confocal laser-scanning microscope (LSM510, Carl Zeiss) at room temperature.

## 5-4 Results and Discussion

To enclose my model system in a lipid layer, CWD that consists of water-phase droplets enclosed in a lipid monolayer and is suspended in oil was used. When common phospholipids (phosphatidylcholine, phosphatidylethanolamine, phosphatidylserine and phosphatidylglycerol) and mixtures (many kinds of combination composed of these phospholipids) were used, actin was dispersed in droplets and interaction between actin and the lipid layer was not observed (data not shown). Because actin is negatively charged (Martonosi *et al.*, 1964; Zimmerle *et al.*, 1987), it is expected that a lipid monolayer with positively charged head groups attracts actin to the inner surface of the lipid layer by electrostatic force. Thus, DOTAP, which is a positively charged amphiphile, was substituted for common phospholipids. As a result, actin was localized at the inner surface of droplets as expected (Figure 1). The concentration of proteins enclosed in droplets influenced on localization of actin. When the proteins concentration derived from cytoplasmic extract was 0.5 mg/ml, some actin accumulated in droplet surface. At 2 mg/ml, accumulation of actin on the surface is the maximum. At protein concentration higher than 5 mg/ml, actin tended to be uniformly distributed in droplets. *In vivo*, actin and cell membrane are connected by proteins, such as ezrin, radixin, moesin, *etc.* (Bretscher *et al.*, 2002; Charras, 2008; Gautreau *et al.* 2000; Fackler & Grosse, 2008). In this DOTAP system, DOTAP plays the role of cell membrane and proteins which bind both actin and cell membrane.

Next, I added the actomyosin fraction to this DOTAP CWD system. In this system, the concentration of proteins derived from the cytoplasmic extract was constant (2 mg/ml). On the other hand, the concentration of proteins derived from

actomyosin fraction was changed. Figure 2 shows typical images of results. When 2 mg/ml actomyosin fraction was used, actin accumulated on droplets surface similarly to using the cytoplasmic extract only. At 10 mg/ml, accumulated actin on surface somewhat decreased, and interestingly the surface of the droplets was rugged. This suggests the droplets become contracted. At concentrations higher 15 mg/ ml, actin tended to be accumulated in center of the droplets. In some previous reports, actin or actomyosin was entrapped in CWD or liposomes (Cortese *et al.*, 1989; Häckl *et al.*, 1998; Hase & Yoshikawa, 2006; Honda *et al.*, 1999; Limozin *et al.*, 2003; Miyata & Hotani, 1992; Miyata *et al.*, 1999; Takiguchi, 1991; Takiguchi *et al.*, 2008, 2011; Tsai *et al.*, 2011). However, surface contraction has not been observed. Since water cannot move beyond the surface of droplets, it is difficult to deform droplets actively. To resolve this problem, this system is enclosed by lipid bilayer, and water of inner membrane is decreased. This is future subject, however, this CWD system will provide a start line to elucidate the mechanism of force generation in bleb-driven amoeboid locomotion, because surface contraction is an important process in generation of motive force in blebbing cell (Charras, 2008; Fackler & Grosse, 2008).

5-5 Figures

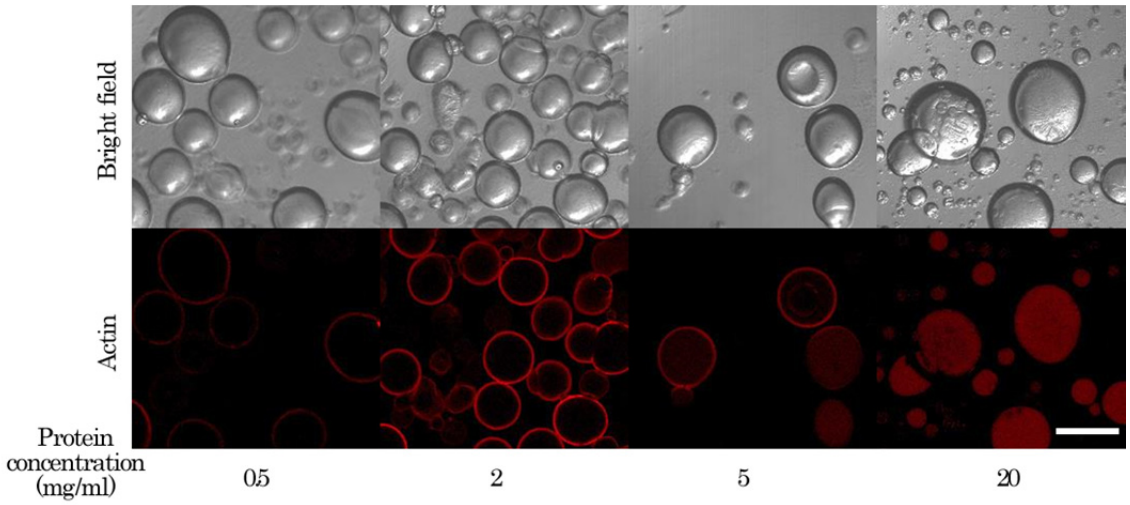


**Figure 1. Accumulation of action on the inner surface of droplets in the CWD system.** Variety concentrations of the cytoplasmic extract were added to mineral oil in which DOTAP was dissolved. Distribution of actin was visualized by staining with rhodamine phalloidin. Scale bar, 200 μm.

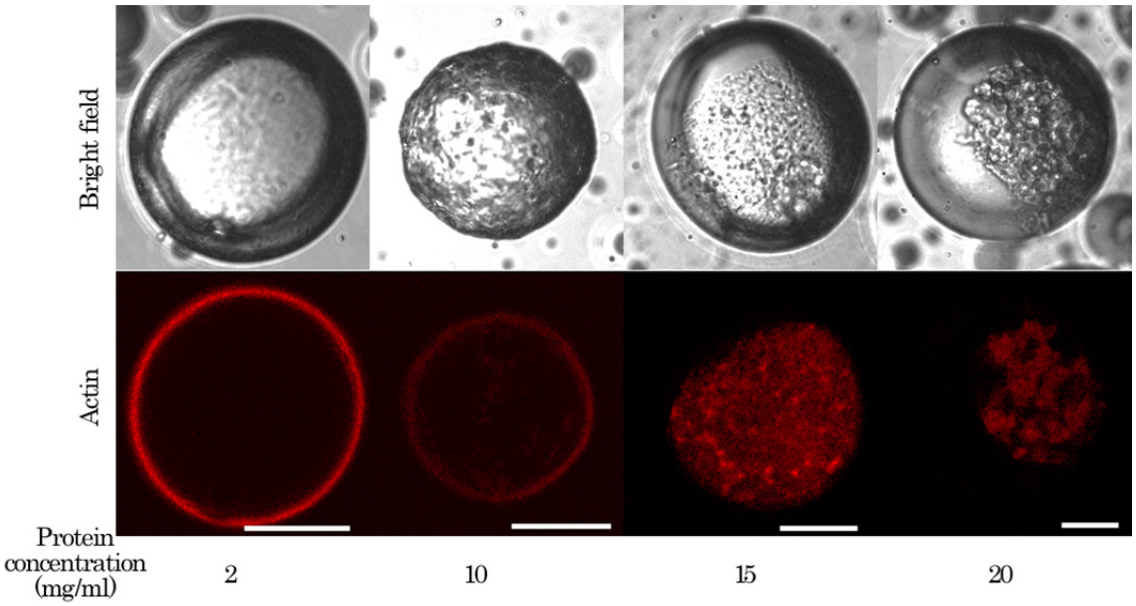


**Figure 2. Addition of the actomyosin fraction altered actin distribution and surface structure of the droplets in the CWD system.** Variety concentrations of the actomyosin fraction were added to mineral oil in which DOTAP was dissolved in the presence of constant concentration of cytoplasmic extract. Distribution of actin was visualized by staining with rhodamine phalloidin. Scale bar, 50 μm.

## Chapter 6 General Discussion

In this thesis, I succeeded in developing two novel model systems to analize amoeboid locomotion of *A. proteus*, the IVA system (Chapter 2) and the CWD system (Chapter 5). The analyses using the IVA system demonstrated that a presence of new mechanism of sol-gel conversion during amoeboid locomotion (Chapter 3). Relation between calcium ion and activities of the IVA system was exhibited by the fact that there is a [$Ca^{2+}$] requirement in the cytoplasmic extract for *in vitro* pseudopod formation, and similar relation was observed in the *in vivo* system (Chapter 4). Previous electron microscopic studies reported the *A. proteus* has an actin meshwork structure under the cell membrane, and the actomyosin meshwork surrounding the endoplasm at intra region of the actin meshwork structure (Sonobe & Kuroda, 1986; Stockem *et al.*, 1982). The IVA system is not enclosed by the cell membrane (Chapter 2), but the actomyosin fraction, the cytoplasmic extract and the boundary surface seem to be equivalent to the endoplasm, the actin mesh structure and the actomyosin meshwork, respectively. Therefore, changes of concentration of calcium ion in the cytoplasmic extract of the IVA system is thought to be equivalent to that in the actin mesh structure *in vivo*. In Chapter 4, I discussed the function of calcium ion focusing on attachment and detachment of the cortex actin fiber and the cell membrane. Now, considering influences of calcium ion on the actin fiber structure, pseudopod formation induced by elevation of calcium ion is explained by deformation and/or solation of the actin meshwork structure. In fact, deformation and solation of the actin meshwork structure is induced by calcium ion *in vitro* in the presence of actin related proteins (Janson & Taylor, 1993), and it was reported that destruction of the cell cortex actin mesh had an ability to induce blebbing, even

if the cell cortex actin attached to the cell membrane (Keller & Eggli, 1998; Paluch *et al.*, 2005). As reviewed by Paluch & Raz (2013), it is difficult to observe the destruction of the cell cortex and detachment of the cell cortex actin from the cell membrane, individually. Therefore, so far, no one has succeeded description of the early events of blebbing. Because the IVA system does not have the cell membrane surrounding the system, the influence of destruction of actin cortex may be interpreted without taking the effects of detachment of the cortical actin from the membrane into account. Thus, I think that destruction of the actin cortex is sufficient to form blebs. Of course, further investigation will be required to reach the final conclusion. Especially, *in vivo* analysis may be required. Since, in *A. proteus*, the destruction of the cell cortex is observed after the detachment of the cell cortex actin from the cell membrane, and these processes are easily to observe separately using differential interference microscope (Mast, 1923, 1926), *A. proteus* is useful to study this phenomena. This study is challenges for the future.

About 50 years ago, two hypotheses, called the front-contraction and tail-contraction hypotheses, were proposed to explain the origin of the motive force of amoeboid movement. Although many experiments supported tail-contraction hypothesis (Goldacre & Lorch, 1950; Goldacre, 1956, 1961, 1964; Jahn, 1964; Kawakatsu *et al.*, 2000; Marsland, 1956; Mast, 1923, 1926; Oh & Jeon, 1998; Rinaldi & Jahn, 1963; Rinaldi *et al.*, 1975; Stockem *et al.*, 1982, 1984; Taylor *et al.*, 1980b; Yanai *et al.*, 1996), the hypothesis could not explain the Allen's observations (Allen, 1961; Allen *et al.*, 1960), which supported front-contraction hypothesis. In his experiments demembraned cell cytoplasm moved in grass capillary despite the fact that the demembraned system would not produce hydrostatic pressure. In

Chapter 2, I demonstrated that, in the IVA system, the actomyosin fraction, which was not enclosed by membrane, could move like amoeba. This phenomenon indicated that some hydrostatic pressure even in the absence of the membrane. Therefore, I conclude that, Allen's argument is irrelevant. The movement of the Allen's system continued for one hour, because of having an ability of relaxation of contracted actomyosin. In the IVA system, this ability is thought to be lost. The mechanisms of relaxation remain to be solved.

Since components can be exchanged arbitrarily in the IVA system and the CWD systems, the systems are thought to be useful to identification of factors essential for bleb-driven amoeboid movement with the help of biochemical techniques. Relevant and urgent issues to be solved to the next stage are to identify minimum components essential to bleb-driven amoeboid locomotion and to understand fundamental modes of individual components for reconstituting the movement with defined components. My IVA and CWD systems will perform great contribution to these issues. My final goal is making liposomes that move like amoeba.

## References

Allen, R. D. A new theory of ameboid movement and protoplasmic streaming. *Exp. Cell Res. Suppl.* **8,** 17-31 (1961).

Allen, R. D., Cooledge, J. W. & Hall, P. J. Streaming in cytoplasm dissociated from the giant amoeba, Chaos chaos. *Nature* **187,** 896-899 (1960).

Blaser, H., Reichman-Fried, M., Castanon, I., Dumstrei, K., Marlow, F. L., Kawakami, K., Solnica-Krezel, L., Heisenberg, C. P. & Raz, E. Migration of zebrafish primordial germ cells: a role for myosin contraction and cytoplasmic flow. *Dev. Cell* **11,** 613-627 (2006).

Boulbitch, A., Simson, R., Simson, D. A., Merkel, R., Häckl, W., Bärmann, M. & Sackmann, E. Shape instability of a biomembrane driven by a local softening of the underlying actin cortex. *Phys. Rev. E* **62,** 3974-3985 (2000).

Bretscher, A., Edwards, K. & Fehon, R. G. ERM proteins and merlin: integrators at the cell cortex. *Nat. Rev. Mol. Cell Biol.* **3,** 586-599 (2002).

Gautreau, A., Louvard, D. & Arpin, M. Morphogenic effects of ezrin require a phosphorylation-induced transition from oligomers to monomers at the plasma membrane. *J. Cell Biol.* **150,** 193-203 (2000).

Charras, G. T. A short history of blebbing. *J. Microsc.* **231,** 466-478 (2008).

Charras, G. T., Hu, C. K., Coughlin, M. & Mitchison, T. J. Reassembly of contractile actin cortex in cell blebs. *J. Cell Biol.* **175,** 477-490 (2006).

Charras, G. T. & Paluch, E. Blebs lead the way: how to migrate without lamellipodia. *Nature Rev. Mol. Cell Biol.* **9,** 730-736 (2008).

Charras, G. T., Yarrow, J. C., Horton, M. A., Mahadevan, L. & Mitchison, T. J. Non-equilibration of hydrostatic pressure in blebbing cells. *Nature* **435,** 365-369 (2005).

Cobbold, P. Cytoplasmic free calcium and amoeboid movement. *Nature* **285,** 441-446 (1980).

Goldstein, H., Poole, C. P. & Safko, J. L. *Classical mechanics* (Addison-Wesley, New York, 2001).

Gollnick, F., Meyer, R. & Stockem, W. Visualization and measurement of calcium transients in Amoeba proteus by fura-2 fluorescence. *Eur. J. Cell Biol.* **55,** 262-271 (1991).

Cortese, J. D., Schwab, B. 3rd, Frieden, C. & Elson, E. L. Actin polymerization induces a shape change in actin-containing vesicles. *Proc. Natl. Acad. Sci. USA.* **86,** 5773-5777 (1989).

Olson, M. F. & Sahai, E. The actin cytoskeleton in cancer cell motility. *Clin. Exp. Metastasis* **26,** 273-287 (2009).

Fackler, O. T. & Grosse, R. Cell motility through plasma membrane blebbing. *J. Cell Biol.* **181,** 879-884 (2008).

Häckl, W., Barmann, M. & Sackmann, E. Shape Changes of Self-Assembled Actin Bilayer Composite Membranes. *Phy. Rev. Lett.* **80,** 1786-1789 (1998).

Hase, M. & Yoshikawa, K. Structural transition of actin filament in a cell-sized water droplet with a phospholipid membrane. *J. Chem. Phys.* **124,** 104903 (2006).

Heald, R., Tournebize, R., Blank, T., Sandaltzopoulos, R., Becker, P., Hyman, A. & Karsenti, E. Self-organization of microtubules into bipolar spindles around artificial chromosomes in Xenopus egg extracts. *Nature* **382,** 420-425 (1996).

Honda, M., Takiguchi, K., Ishikawa, S. & Hotani, H. Morphogenesis of liposomes encapsulating actin depends on the type of actin-crosslinking. *J. Mol. Biol.* **287,** 293-300 (1999).

Ishiwata, S. & Yasuda, K. Mechanochemical coupling in spontaneous oscillatory contraction of muscle. *Phase Transitions* **45,** 105-136 (1993).

Janson, L. & Taylor, T. D. In vitro models of tail contraction and cytoplasmic streaming in amoeboid cells. *J. Cell Biol.* **123,** 345-356 (1993).

Kato, A., Shindo, E., Sakaue, T., Tsuji, A. & Yoshikawa, K. Conformational transition of giant DNA in a confined space surrounded by a phospholipid membrane. *Biophys. J.* **97,** 1678-1686 (2009).

Kawakatsu, T., Kikuchi, A., Shimmen, T. & Sonobe, S. Interaction of actin filaments with the plasma membrane in Amoeba proteus: studies using a cell model and isolated plasma membrane. *Cell Struct. Funct.* **25,** 269-277 (2000).

Keller, H. & Eggli, P. Protrusive activity, cytoplasmic compartmentalization, and restriction rings in locomoting blebbing Walker carcinosarcoma cells are related to detachment of cortical actin from the plasma membrane. *Cell Motil. Cytoskeleton* **41,** 181-193 (1998).

Keller, H., Rentsch, P. & Hagmann, J. Differences in cortical actin structure and dynamics document that different types of blebs are formed by distinct mechanisms. *Exp. Cell Res.* **277,** 161-172 (2002).

Kohno, T. & Shimmen, T. Accelerated sliding of pollen tube organelles along Characeae actin bundles regulated by $Ca^{2+}$. *J. Cell Biol.* **106,** 1539–1543 (1988).

Kunita, I., Sato, K., Tanaka, Y., Takikawa Y, Orihara, H. & Nakagaki, T. Shear

Banding in an F-actin Solution. *Phys. Rev. Lett.* **109,** 248303 (2012).

Kuroda, K. & Sonobe, S. Reactivation of a glycerinated model of amoeba. *Protoplasma* **109,** 127-142 (1981).

Kuroda, K., Yoshimoto, Y. & Hiramoto, Y. Temporal and spatial localization of $Ca^{2+}$ in moving Amoeba proteus visualized with aequorin. *Protoplasma* **144,** 64-67 (1998).

Lee, K., Gallop, J. L., Rambani, K. & Kirschner, M. W. Self-assembly of filopodia-like structures on supported lipid bilayers. *Science* **329,** 1341-1345 (2010).

Limozin, L., Bärmann, M. & Sackmann, E. On the organization of self-assembled actin networks in giant vesicles. *Eur. Phys. J. E* **10,** 319-330 (2003).

MacLean-Fletcher, S. D. & Pollard, T. D. Viscometric analysis of the gelation of Acanthamoeba extracts and purification of two gelation factors. *J. Cell Biol.* **85,** 414-428 (1980).

Mahadevan, L. & Pomeau, Y. Rolling droplets. *Phys. Fluids* **11,** 2449-2453 (1999).

Marion, S., Guillen, N., Bacri, J. C. & Wilhelm, C. Acto-myosin cytoskeleton dependent viscosity and shear-thinning behavior of the amoeba cytoplasm. *Eur. Biophysics J.* **34,** 262-272 (2005).

Martonosi, A., Molino, C. M. & Gergely, J. The binding of divalent cations to actin. *J. Biol. Chem.* **239,** 1057-1064 (1964).

Mast, S. O. Mechanics of locomotion in amoeba. *Proc. Natl. Acad. Sci. USA.* **9,** 258-261 (1923).

Mast, S. O. Structure, movement, locomotion, and stimulation in amoeba. *J. Morphol. Physiol.* **41,** 347-425 (1926).

Maugis, B., Brugués, J., Nassoy, P., Guillen, N., Sens, P. & Amblard, F. Dynamic instability of the intracellular pressure drives bleb-based motility. *J. Cell Sci.* **123,** 3884-3892 (2010).

Merkel, R., Simson, R., Simson, D. A., Hohenadl, M., Boulbitch, A., Wallraff, E. & Sackmann, E. A micromechanic study of cell polarity and plasma membrane cell body coupling in Dictyostelium. *Biophys. J.* **79,** 707-719 (2000).

Mitchison, T. J. & Cramer, L. P. Actin-based cell motility and cell locomotion. *Cell* **84,** 371-379 (1996).

Miyata, H. & Hotani, H. Morphological changes in liposomes caused by polymerization of encapsulated actin and spontaneous formation of actin bundles. *Proc. Natl. Acad. Sci. USA.* **89,** 11547-11551 (1992).

Miyata, H., Nishiyama, S., Akashi, K. & Kinosita, K. Protrusive growth from giant liposomes driven by actin polymerization. *Proc. Natl. Acad. Sci. USA.* **96,** 2048-2053 (1999).

Murray, A. & Kirschner, M. Cyclin synthesis drives the early embryonic cell cycle. *Nature* **339,** 275-280 (1989).

Nagel, G., Szellas, T., Huhn, W., Kateriya, S., Adeishvili, N., Berthold, P., Ollig, D., Hegemann, P. & Bamberg, E. Channelrhodopsin-2, a directly light-gated cation-selective membrane channel. *Proc. Natl. Acad. Sci. USA.* **100,** 13940-13945 (2003).

Nishihara, E., Yokota, E., Tazaki, A., Orii, H., Katsuhara, M., Kataoka, K., Igarashi, H., Moriyama, Y., Shimmen, T. & Sonobe, S. Presence of aquaporin and V-ATPase on the contractile vacuole of Amoeba proteus. *Biol. Cell.* **100,** 179-188 (2008).

Oh, S. W. & Jeon, K. W. Characterization of myosin heavy chain and its gene in Amoeba proteus. *J. Eukaryot. Microbiol.* **45,** 600-605 (1998).

Paluch, E., Piel, M., Prost, J., Bornens, M. & Sykes, C. Cortical actomyosin breakage triggers shape oscillations in cells and cell fragments. *Biophys. J.* **89,** 724-733 (2005).

Paluch, E., Sykes, C., Prost, J. & Bornens, M. Dynamic modes of the cortical

actomyosin gel during cell locomotion and division. *Trends Cell Biol.* **16,** 5-10 (2006).

Paluch, E. K. & Raz, E. The role and regulation of blebs in cell migration. *Curr. Opin. Cell Biol.* **25,** 1-9 (2013).

Parent, C. A. Making all the right moves: chemotaxis in neutrophils and Dictyostelium. *Curr. Opin. Cell. Biol.* **16,** 4-13 (2004).

Pollard, T. D. & Borisy, G. G. Cellular motility driven by assembly and disassembly of actin filaments. *Cell* **112,** 453-465 (2003).

Rentsch, P. S. & Keller, H. Suction pressure can induce uncoupling of the plasma membrane from cortical actin. *Eur. J. Cell Biol.* **79,** 975-981 (2003).

Rinaldi, R. & Opas M. Graphs of contracting glycerinated Amoeba proteus. *Nature* **260,** 522-526 (1978).

Rogers, S. S., Waigh, T. A. & Lu, J. R. Intracellular microrheology of motile Amoeba proteus. *Biophys. J.* **94,** 3313-3322 (2008).

Sanchez, T., Welch, D., Nicastro, D. & Dogic, Z. Cilia-like beating of active microtubule bundles. *Science* **333,** 456-459 (2011).

Sonobe, S. & Kuroda, K. Ultrastructural aspects of a glycerinated model of Amoeba

proteus. *Protoplasma* **50,** 41-50 (1986).

Stockem, W., Hoffmann, H. U. & Gawlitta, W. Spatial organization and fine structure of the cortical filament layer in normal locomoting Amoeba proteus. *Cell Tissue Res.* **221,** 505-519 (1982).

Stockem, W. & Klopocka, W. Amoeboid movement and related phenomena. *Int. Rev. Cytol.* **112,** 137-183 (1988).

Stockem, W., Naib-Majani, W. & Wohlfarth-Bottermann, K. E. Preservation and phallotoxin-staining of the microfilament system in Amoeba proteus. *Cell Biol. Int. Rep.* **8,** 207-213 (1984).

Takiguchi, K. Heavy meromyosin induces sliding movements between antiparallel actin filaments. *J. Biochem.* **527,** 520-527 (1991).

Takiguchi, K., Negishi, M., Tanaka-Takiguchi, Y., Homma, M. & Yoshikawa, K. Transformation of ActoHMM assembly confined in cell-sized liposome. *Langmuir* **27,** 11528-11535 (2011).

Takiguchi, K., Yamada, A., Negishi, M., Tanaka-Takiguchi, Y. & Yoshikawa, K. Entrapping desired amounts of actin filaments and molecular motor proteins in giant liposomes. *Langmuir* **24,** 11323-11326 (2008).

Taylor, D. T., Blinks, J. & Reynolds, G. Contractile basis of amoeboid movement. VII. Aequorin luminescence during ameboid movement, endocytosis, and capping. *J. Cell biol.* **86,** 599-607 (1980a).

Taylor, D. L., Wang, Y. L. & Heiple, J. M. Contractile basis of ameboid movement. VII. The distribution of fluorescently labeled actin in living amebas. *J. Cell Biol.* **86,** 590-598 (1980b).

Tinevez, J. Y., Schulze, U., Salbreux, G., Roensch, J., Joanny, J. F. & Paluch, E. Role of cortical tension in bleb growth. *Proc. Natl. Acad. Sci. USA.* **106,** 18581-18586 (2009).

Toyota, T., Head, D. A., Schmidt, C. F. & Mizuno, D. Non-Gaussian athermal fluctuations in active gels. *Soft Matter* **7,** 3234-3239 (2011).

Tsai, F. C., Stuhrmann, B. & Koenderink, G. H. Encapsulation of active cytoskeletal protein networks in cell-sized liposomes. *Langmuir* **27,** 10061-10071 (2011).

van der Gucht, J. & Sykes, C. Physical model of cellular symmetry breaking. *Cold Spring Harbor Perspect. Biol.* **1,** a001909 (2009).

Yanai, M., Kenyon, C. M., Butler, J. P., Macklem, P. T. & Kelly, S. M. Intracellular pressure is a motive force for cell motion in Amoeba proteus. *Cell Motil. Cytoskeleton* **33,** 22-29 (1996).

Yoshida, K. & Soldati, T. Dissection of amoeboid movement into two mechanically distinct modes. *J. Cell Sci.* **119,** 3833-3844 (2006).

Zhao, M. Electrical fields in wound healing-An overriding signal that directs cell migration. *Semin. Cell Dev. Biol.* **20,** 674-682 (2009).

Zimmerle, C. T., Patane, K. & Frieden, C. Divalent cation binding to the high- and low-affinity sites on G-actin. *Biochemistry* **26,** 6545-6552 (1987).

## Acknowledgement